

Disentangling of spectra – theory and practice

P. Hadrava,

Astronomical Institute, Academy of Sciences of the Czech Republic,
Boční II 1401, 141 31 Praha 4, Czech Republic

e-mail: had@sunstel.asu.cas.cz

<http://www.asu.cas.cz/~had/korel.html>

Release September 19, 2008

modified August 31, 2009

Abstract

In this document a review of the author's method of Fourier disentangling of spectra of binary and multiple stars is presented for the purpose of the summer school organized at Ondřejov observatory in September 2008. Related methods are also discussed and some practical hints for the use of the author's code KOREL and related auxiliary codes with examples are given.

keywords: Spectroscopic binaries and multiple stars – orbital elements – line profiles – spectra disentangling

Contents

Introduction	3
1 Theory of spectra disentangling	7
1.1 A swift entry into the theory	7
1.2 Background thoughts	10
1.3 Methods of radial-velocity measurements	14
1.3.1 Method of cross-correlation	14
1.3.2 Method of broadening function	17
1.4 Methods of decomposition of spectra	18
1.4.1 Direct subtraction	18
1.4.2 Iterative subtraction	19
1.4.3 Method of tomographic separation	20
1.5 Method of wavelength-domain disentangling of spectra	23
1.6 Fourier disentangling and its generalizations	25
1.6.1 Principle of Fourier disentangling	25
1.6.2 Simple Fourier disentangling	27
1.6.3 Line-strength variations and removal of telluric lines	29
1.6.4 Line photometry	32
1.6.5 Disentangling with intrinsic line-profile variations	35
1.6.6 Broadening by pulsations	37
1.6.7 Rotational (Schlesinger – Rossiter – McLaughlin) effect	38
1.6.8 Disentangling with constraints	40
1.6.9 Discretization of the input spectra	41
1.6.10 Normalization of disentangled spectra	44
1.6.11 Numerical method	47
2 Practice of spectra disentangling	101
2.1 Practical conditions for the use of KOREL	101
2.2 An easy start with KOREL	103
2.2.1 Example 1 – simulated data	103
2.2.2 Example 2 – 96 Her	107
2.2.3 Example 3 – 55 UMa	108

2.3	Rectification of the input spectra	109
2.3.1	Example 4 – α CrB	109
2.3.2	Example 5 – 68 u Her	109
A	Appendices	201
A.1	Historical background	201
A.2	Mathematical background	203
A.2.1	Fourier transform	203
A.2.2	Radon transform	204
A.2.3	Moments of functions	207
A.3	Manual for users of KOREL	208
A.3.1	Implementation of the code	208
A.3.2	Controlling the run (file <code>korel.par</code>)	208
A.3.3	Input data (file <code>korel.dat</code>)	211
A.3.4	The code PREKOR	211
A.3.5	The code REKTIF	214
A.3.6	The code KORTTRANS	215
A.3.7	Input data (file <code>korel.tmp</code>)	216
A.3.8	Outputs of KOREL	216
A.3.9	The code KORNOR	218
A.3.10	Problems with KOREL	218
A.4	List of objects studied with Fourier disentangling	220
	References	221
	Program of the Summer School	225
	List of participants	226

Introduction

Observations of binary and multiple stars enable us to determine their basic physical parameters which are not so easily reachable for single stars. This is why, in spite of their more complicated physics, the binaries are a clue to understanding the physics, structure and evolution of stars in general. This knowledge is then a basis for understanding the physics of higher systems (clusters of stars and nebulae of interstellar matter, galaxies, as well as the Universe as a whole). Observations of binaries can also be used as a primary method of distance determination.

Different methods of observations of binaries are complementary and should be used simultaneously to combine and exploit optimally their sensitivities to different parameters of the observed systems. The spectroscopic observations reveal the variations of Doppler-shifts of spectral lines of the component stars caused by changes of radial velocities in the course of the orbital motion. (The conception of spectroscopic radial velocity only seems to be straightforward – for its definition and discussion see, e.g., Lindegren and Dravins 2003). In combination with inclination of the orbital plane which can be found e.g. from a light-curve solution for eclipsing binaries, radial velocities yield the orbital velocity and thus also the information on absolute dimensions of the orbit. Using the third Kepler law also the masses of the stars can be determined and attributed to the spectral types of the stars. This, however, requires to distinguish spectral features belonging to the individual component stars, i.e. to decompose the observed superposition of the light of the components into the individual spectra of the component stars. This decomposition can be performed by comparison of spectra taken at different known radial velocities of the individual components or at phases with different known light ratios of the components (e.g. during eclipses) or with some other well established variations of the component spectra. Because the information on the component spectra as well as on the radial velocities or the orbital and other parameters of the observed system is entangled in the observed spectra, the procedure of solution for this information is referred to as the “disentangling” – cf. Fig. 1. Such a method of solving for orbital parameters and simultaneous decomposition of spectra of binaries was first published (and named) by Simon and Sturm (1994) who used the method of singular-value decomposition (SVD) in the wavelength domain to separate the component spectra.

The method by Simon and Sturm turned out to be in principle (by the formulation of the problem and by its properties) equivalent to the method which I developed from the method of cross-correlation for radial velocity measurements between 1990 and 1993. The aim of this my work was originally to enable measurement of radial velocities of highly blended lines of the components (i.e. at phases close to conjunctions, but also practically at all phases for wide lines of early type stars with small amplitudes of radial velocities). I realized soon that it would be advantageous to skip the step of determination of radial velocities and to include instead of it directly the observed spectra. These spectra could thus be another possible input for the code FOTEL which I designed

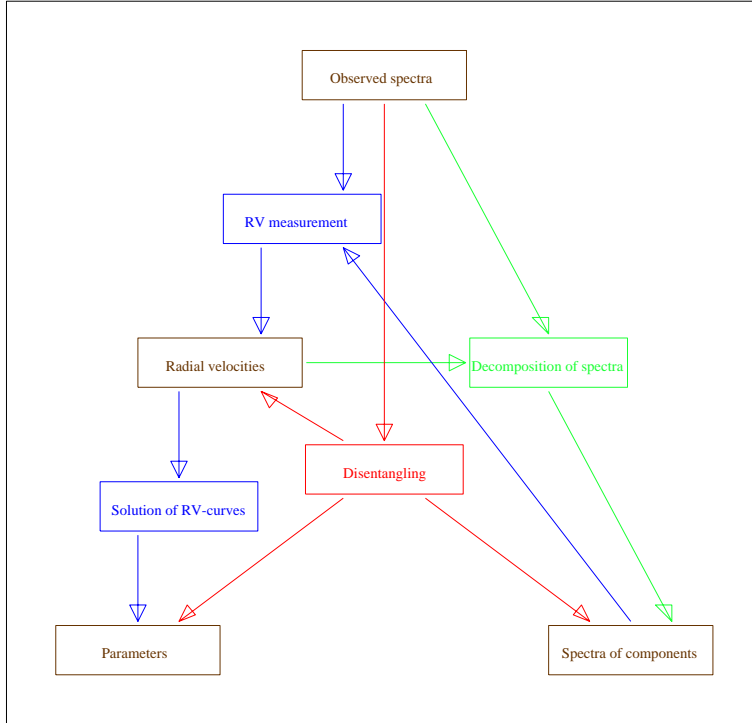


Figure 1: A scheme of disentangling method compared with the classical processing of spectra of binary stars: orbital parameters are determined from the observed spectra with an intermediate step of radial-velocity measurement (blue), spectra of components may be separated using known radial velocities (green), while in disentangling all unknown quantities are determined together as the best fit of the observations

originally for solution of light-curves (i.e. determination orbital ELements from the FO-Tometry), and which I enriched also for a simultaneous solution of radial velocity curves (for which also the code SPE(ctroscopic)EL(ements) was written by Jiří Horn) and later also for astrometric/interferometric data. The incorporation of cross-correlation should avoid measurements of radial velocities and it is this relation with the cross-correlation why I renamed the corresponding code KOR(elation)EL(ements) from its original name BAŽANT (which means pheasant whose colours were resembled by the curves on the screen) given to it by my son (who used then to help me at his age of three years). My additional intention was to improve the method of cross-correlation by cross-correlating mutually spectra of the same system obtained at different phases instead of correlating each exposure with an arbitrarily chosen template. To distinguish which peak in cross-correlation is due to which combination of components, it turned out to be preferable to decompose the spectra. The formulation of the problem in this complexity was later defined (which means that it was developed practically at the same time) by Simon and Sturm (1994) as the disentangling. Such a decomposition of spectra is relatively easy in Fourier representation, which is commonly used in the cross-correlation, but it qualitatively surpasses the original cross-correlation in the sense explained by Rucinski (2002). At the same time, the Fourier disentangling is numerically much more efficient than the wavelength-domain disentangling. This efficiency enables a further generalization of the method (e.g. to include easily more components).

Similarly as before with the code FOTEL, I made from the very beginning the source-file of the KOREL-code publicly available first on FTP and then on my web-pages. For a convenience of users, I published in an electronic form on the web also reviews of the methods and manuals for the use of FOTEL and KOREL, which I upgraded and supplemented simultaneously (or with some delay or advance) with the development of the codes and publications of the news in the literature. While skilled users appreciated this practice, some other disabled it by misusing the texts and spreading of various desinformations. The versions of the codes FOTEL and KOREL from the year 2004, when also their descriptions were printed are thus the last made available. Because these versions of 2004 are already obsolete it is no more worth to support them.

In the mean time, several users in the world reached very good results applying the method of Fourier disentangling and the KOREL code for particular stellar systems. There is an increasing audience of astrophysicists willing to use the method, but some of them meet problems in the beginning or they do not use it in an optimal way. Frequent requests for a help with the use of disentangling gave rise to the idea to organize a summer school, in which the theory of the method as well as the practice with the code KOREL will be explained.

In comparison with the version of KOREL of 2004, the new version of 2008 is much more powerful in its precision and efficiency. This is why I prefer to deal with the new one, in spite of suggestions that even the old one is not yet properly understood. The new version also enables some new options. Fortunately, the previously available possibilities are still controlled basically in the same way as in the version of 2004, despite it will be probably necessary to change in some way in near future. Until such a version will be prepared, verified and properly described, a technical solution is to provide users with a remote access to computer of the Astronomical Institute with a compiled version of KOREL08, where they could disentangle their spectra in the way which will be shown in this summer school.

The present document is a preprint of textbook on the method of Fourier disentangling and related topics from physics of binaries. It is provided for a personal use of participants of the school with a warning that it is still a very preliminary version. It explains in details some theoretical aspects of the method in Chapter 1 and provides a practical experience in the use of its implementation in the code KOREL in Chapter 2. It is based on the previous review of the method (Hadrava 2004c) but it includes some later results including some quite recent, which will be published elsewhere. Partly updated manual on KOREL from the same publication is included in Appendix together with some other auxiliary resources.

To save the time and to enable practical exercises from the very beginning of the course, I shall explain first the simplest version of the method of Fourier disentangling in Section 1.1 and the use of the KOREL code in Section 2.2. However, a thorough understanding of the theoretical background is needed for a safe use of the method, not to say for its further development. We shall thus return in subsequent Sections to different,

in some cases even very general topics, which, from the purely logical point of view should precede.

Chapter 1

Theory of spectra disentangling

1.1 A swift entry into the theory

Let us suppose that a multiple stellar system consists of n stars and that the intrinsic spectrum $I_j(x)|_{j=1}^n$ of each component is constant in time (i.e. it has no intrinsic physical or geometric variability) apart of being Doppler-shifted according to the instantaneous radial velocity $v_j(t)$ of the star j at the time t . As it is customary, here we use x as an independent variable of the spectrum, the logarithmic wavelength scale

$$x = c \ln \lambda , \quad (1.1)$$

in which the Doppler shift is the same for all frequencies. For instance, for a radial velocity $v \ll c$ much smaller than the speed of light the non-relativistic approximation gives

$$v = c \Delta \lambda / \lambda = \Delta x , \quad (1.2)$$

while the relativistic formula

$$\Delta x(v) = c \ln \frac{\sqrt{c^2 - v^2 - v_\perp^2}}{c - v} \quad (1.3)$$

(where v_\perp is the tangential component of the velocity) is non-linear in v but still independent on λ equally as the general-relativistic red-shifts.¹

According to Eq. (1.2), the observable spectrum of the star j is given by convolution with shifted Dirac delta-function $\delta(x - v_j(t))$ and the composite spectrum of the whole stellar system observed at time t is the superposition of these convolutions²

$$I(x, t) = \sum_{j=1}^n I_j(x) * \delta(x - v_j(t)) . \quad (1.4)$$

¹This could be violated by a dispersive medium between the source and observer.

²In fact the Doppler shift modifies also the value of intensity depending on the way of its normalization, however, we shall mostly use the rectified spectra, i.e. ratios of the actual spectra and their continua.

Comparing such spectra obtained at different times, we would like to find what is common for all of them, i.e. the spectra $I_j(x)$ of the components, and what is changing, i.e. the instantaneous radial velocities $v_j(t)$. Obviously, without any additional conditions (e.g. on smoothness of $I_j(x)$ or its shape) such a solution is in principle possible if we have N ($N > n$) spectra $I(x, t_l)$ taken in suitable times $t_l|_{l=1}^N$ at different radial velocities. Typically, the observed spectra are sampled in number of bins of the order of thousands. With a few unknown radial velocities (or orbital parameters by which the radial velocities are bound), the solving for all the unknown variables is overdetermined already if $n + 1$ observed spectra are taken into account. However, because each exposure includes also some noise, it is desirable to treat even more observations at once and to fit them simultaneously by all the unknowns – both the component spectra as well as the radial velocities or some other relevant parameters.

Assuming first the radial velocities to be known, Eq. (1.4) is a huge set of linear equations coupled for all wavelengths (provided differences between $v_j(t)$ vary with t). The inversion of the corresponding large (but sparse) matrix can be simplified in a suitable representation, in which the operator separates into smaller submatrices (cf. the experience from quantum mechanics). Really, Fourier transform provides such a representation, because it changes the convolution of functions to a simple product of their Fourier modes. Fourier transform ($x \rightarrow y$) of Eq. (1.4) reads

$$\tilde{I}(y, t) = \sum_{j=1}^n \tilde{I}_j(y) \exp(iy v_j(t)) , \quad (1.5)$$

which really simplifies the task essentially, because the huge set of linear equations splits now into many simple systems of dimension n , i.e. the number of components in the observed system. In this set of equations, independent for each Fourier mode and labeled by the new independent variable y , the expressions $\exp(iy v_j(t))$ are multipliers (known as simple functions of the fixed radial velocities $v_j(t)$) of the component spectra's unknown modes $\tilde{I}_j(y)$, which are to be solved to fit the Fourier modes $\tilde{I}(y, t)$ of the observed spectra. For the simple case of a double-lined spectroscopic binary $n = 2$ the decomposition of spectra simplifies to the solution of $N/2$ ($\frac{1}{2}$ is due to the symmetry) sets of complex linear equations for two unknowns, one in each Fourier mode. It is immediately obvious from Eq. (1.5) that for $y = 0$ this set of equations is singular ($\tilde{I}(y, t) = \sum_{j=1}^n \tilde{I}_j(y)$), it means that in practice the ratio of continua cannot be determined from the Doppler shifts only.

Owing to the Parseval theorem (A.5), the squares of residuals in the wavelength domain x are equal (or proportional depending on the chosen normalization of the Fourier transform) to the residual in the domain of Fourier frequencies y . These residuals ($O - C$) of the observed spectra can thus be minimized by the least-squares method also with respect to the unknown radial velocities $v_j(t_l)$ or directly with respect to the orbital parameters which determine these velocities. This optimization with respect to the parameters is the procedure which complements the above described method of decomposition to become a method of disentangling of the spectra.

Generally, the dependence of the squared residuals of spectra on these parameters is not quadratic (unlike the dependence on the component spectra), so the minimization of the residuals with respect to these parameters must be performed by some general method (e.g. the simplex method used in the KOREL code). This also implies directly, that there may exist some local minima and hence multiple solutions. Some of these solutions may be fully or nearly equivalent (e.g. solutions which refer to different epochs of the periastron passage or with different combinations of periastron longitude and epoch for very small eccentricities), but some may be artifacts of incorrect minimization or of errors or gaps in the data.

1.2 Background thoughts

A short cut leading readers directly *in medias res* of the method of disentangling has been described in the Sections 1.1 and 2.2. The purpose of the present Section is to warn the readers against taking such a way. Instead, let us return first to a very general, rather philosophical principles of the methodology of science. It is commonly accepted, that a progress in development of science is usually achieved by combining experimental (in astronomy it means observational) and theoretical approaches. A routine application of an experimental method without taking into account its theoretical background threatens with an incorrect interpretation of the data.

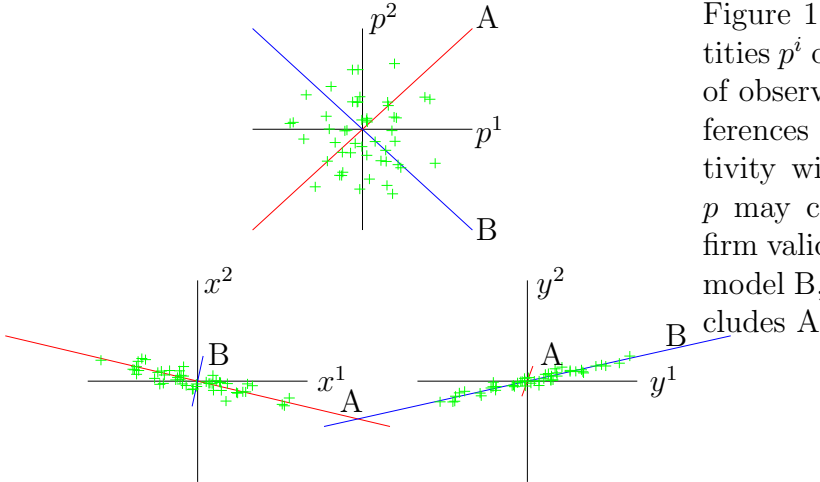


Figure 1.1: Variable physical quantities p^i of a source lead to variations of observable quantities x^k, y^k . Differences between x and y in sensitivity with respect to subspaces of p may cause that x seems to confirm validity of model A and exclude model B, while y confirms B and excludes A

To illustrate the danger of pure observational approach which is seemingly independent of theory or even capable of deciding which theoretical model is correct, let us assume an object, the state of which is described by a set of parameters p^i . In our case the object may be a star and the parameters quantities like density, velocity, pressure, chemical composition, ionization state, magnetic field etc. in different parts of the star. Our observations of the object usually do not allow us to measure directly p^i , but some observable quantities $x^k = x^k(p^i)$ which are their functions. In astrophysics, these quantities are mostly intensities of light in different wavelength bands, polarization states etc. and they reflect the parameters owing to a complex process of radiative transfer. The parameters p^i are mutually linked by physical laws, so that only a few of them are free parameters and have to be determined from the observation. The dependence of the observed quantities x^k on p^i is also a matter of corresponding physics of the observed object, but also of the detecting instrument and the interlying medium, which usually contributes by some noise. The theory of the observed object consists first in the proper choice of its model

and the proper physics governing relations of p^i as well as $x^k(p^i)$ and than in a technical problem to calculate p^i and x^k for chosen values of the free parameters, eventually to solve the inverse problem and determine the free parameters from the observed quantities. The observation of the object consists first in real getting of the values x^k and its aim is to interpret the observations by comparing the observed values with the theoretical predictions and hopefully to decide which theoretical model with which values of free parameters corresponds better to the observational results. However, even a very simplified model illustrated in Fig. 1.1 reveals, that the commonly used practice of best fit (which is also basis of the disentangling) need not be at all a good fit, if the theoretical model is not appropriate or the data are not sufficiently sensitive to parameters to be determined. The upper diagram shows a two-dimensional subspace of parameters p^i centered at their mean values for the object. Assume the object to be perturbed by some process (e.g. a star oscillates around its equilibrium state, or it is affected by magnetic field) and the parameters change for values δp^i . Different theoretical models (e.g. model A and B) of the perturbations may predict different bounds $F(\delta p^i) = 0$ of the perturbations (drawn in the Figure by the skew lines $\frac{\partial F}{\partial \delta p^i} \delta p^i = 0$). These perturbations of the object result in perturbations of observed quantities $\delta x^k = \frac{\partial x^k}{\partial p^i} \delta p^i$ and the models are represented by (generally) different lines also in the space of the observed quantities δx^k . In Fig. 1.1, random uncorrelated perturbations of δp^i (drawn by crosses) are chosen, which suggest that neither model A nor B is a sufficient explanation of the process of perturbations (or that both processes described by these models take place simultaneously). However, different observed quantities $x^k(p^i)$ and $y^k(p^i)$ (in the left and right bottom diagrams, resp.) may be sensitive to different subspaces of δp^i and each one of them seems to be a convincing observational proof of one of the models and an elimination of the other, but their evidence is mutually opposite. The problem seems to be trivial, if the quantities p^i or x^k are of similar nature, so that their scaling could be compared. However, if p^1 and p^2 are, e.g., density and temperature, resp., and x^1 and x^2 magnitude and radial velocity, there is no way to judge if the transform $x^k(p^i)$ is distorted similarly as the left or right diagram.

It follows from this example that the value of observational evidence depends on the class of tested theoretical models as well as on the quality of the data and the method of data processing. It is preferable to take into account a wider variety of data, but even then a good agreement with a theoretical model is not a guaranty that another model is not better. Let us note that in stellar spectroscopy the directly observed quantities are usually the fluxes in different wavelength channels, while radial velocities are already an intermediate result of an interpretation of the spectra, which is biased by several assumptions on the observed source and the instrumentation. For instance, it is obvious that a solution of radial velocity curve will lead to an underestimate of K -velocity if it is smaller than the width of line, which is blended by an unresolved weak line of secondary component, so that the radial velocities measured classically (e.g. by means of moments

of line-profile) are in fact a weighted mean between primary and secondary component. It is thus preferable to fit directly the spectra using the disentangling instead of fitting radial-velocity curve in which the reliability of individual data points is questionable. It is also known that the measured radial velocity curves may be deflected from the simple Keplerian form due to phase-dependent line-profile asymmetries caused by the proximity effects (reflection, tidal distortions etc.). Theoretically estimated corrections are used for the radial-velocity curves, however, for the disentangling it is needed to model directly the line-profile distortions.

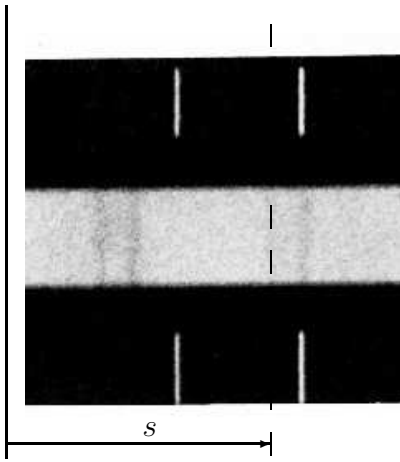


Figure 1.2: Part of Ondřejov spectrogram No. 5197 of double-line binary 96 Her. Wavelength scale is defined by (emission) comparison spectrum exposed on both sides of the stellar (absorption) spectrum in the central horizontal belt

Let me illustrate this problem by a practical experience which is behind the development of my codes FOTEL and KOREL. In 1969 I was asked by my supervisor S. Kříž to investigate the precision of measurement of radial velocities from photographic spectrograms taken with the (then new) Ondřejov 2m-telescope and to elaborate an optimal method. The classical method was the measurement of positions s of stellar and comparison lines fitted visually by a line in microscope of Abbe comparator – cf. Fig. 1.2. (The measurement was very laborious and for tens of lines measured in two directions and two orientations of the plate it took usually a whole day for one plate.) The wavelength scale λs was then calculated by least-squares fit to the positions s_i of all measured comparison lines with known wavelengths λ_i to minimize the influence of errors in measurement of individual lines. For the fit a polynomial approximation

$$\lambda(s) \simeq \sum_{k=0}^m a_k s^k \quad (1.6)$$

was usually accepted, because it was computationally straightforward. The problem was that for a small degree of the polynome (e.g. $m = 3$) the curve was not elastic enough to follow the dispersion curve λs with sufficient precision, and for higher degrees it was too much elastic and the new degrees of freedom were misused by the code to fit individual errors in some lines, which caused large deflections of the curve in regions, where suitable

comparison lines were missing. This is also an example, where a more sophisticated theoretical model is needed for correct interpretation of the measured data to restrict unrealistic degrees of freedom. Such a model is given by the grating angular dispersion

$$\lambda = \frac{d}{n}(\sin \alpha + \sin \beta) , \quad (1.7)$$

where d is the constant of grating, n is the order of spectrum, α the angle of incidence (fixed by configuration of the spectrograph) and $\beta = \beta(s)$ is the angle of diffraction joined with the measured position s of a line by the projection properties of the spectrograph camera. In the case of Ondřejov spectrograph (with bent spectrogram photoplates) it could be well approximated as $\beta = (s - s_0)/f$, where f is the focal length of the camera, the desired model is thus

$$\lambda = b_0 + b_1 \sin(b_3 s - b_2) , \quad (1.8)$$

which should fit the relation $\lambda(s)$ with high precision with just four free parameters (like the polynome of the third degree). A disadvantage with the then available computer (type MINSK with about 20kB of memory but extending in our present lecture-room) was that unlike Eq. (1.6) linear in a_k , Eq. (1.8) is non-linear with respect to coefficients b_2 and b_3 . Generally, the equations

$$0 = \frac{\partial}{\partial p_k} S(p) = \frac{\partial}{\partial p_k} \sum_i (y_i - F(x_i, p))^2 , \quad (1.9)$$

which give the condition of minimum with respect to parameters p of summed squares of residuals of measurements $\{(x^i, y^i)|_{i=1}^n\}$ are linear in p if the function F of the model $y = F(x, p)$ is linear in p , i.e. if F can be expressed as a linear combination of some functions f_k , i.e. $F(x, p) = \sum_k p_k f_k(x)$. It is thus advantageous to rewrite Eq. (1.8) in the form

$$\lambda = c_0 + c_1 \sin(c_3 s) + c_2 \cos(c_3 s) , \quad (1.10)$$

which is linear in c_0 , c_1 and c_2 and non-linear in $c_3 = 1/f$ only. The minimization with respect to the linear coefficients can thus be performed by solution of the set of linear equations and by a computationally more expensive sampling with respect to the non-linear parameter only (which is, moreover, well known in this case). A similar linearization in γ and K -velocity helped to speed up the solution of radial-velocity curve in FOTEL code and it is also the clue to the efficiency of Fourier disentangling.

1.3 Methods of radial-velocity measurements

In the previous Section the determination of radial velocities using classical Abbe comparator was described as an example of different possibilities of numerical treatment of the measured data. The method of measurement and its necessary instrumentation has been improved in many variants. Especially the problem of determination of suitable center of line was attacked using different devices and the corresponding data-processing which enable to display the line-profiles (sometimes together with their mirror images) – e.g. osciloscopic machine (Hossack 1952, cf. Fig. 1.3), tracings (Heinzel and Hadrava 1975), TV-technique (Minaroviech et al. 1984), scans (Škoda 1996). In this Section we shall deal with some techniques of radial-velocity measurement which are related to the method of disentangling. My intention of this description is not to teach how to use those methods (readers are referred to the original works in this respect), but to compare the various approaches and to learn from them in which respect the disentangling should be improved.

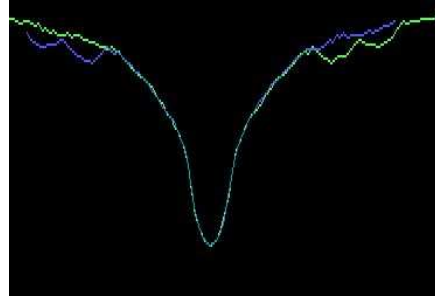


Figure 1.3: Radial velocity measurement by oscilloscopic method

1.3.1 Method of cross-correlation

The idea of this method is based on the fact that the presence of a weak signal of particular type, like is the spectrum of a faint secondary component, blended with a stronger signal or hidden in a noise can be better revealed from overall coincidence with the observed signal than from some local features (cf. Fig. 1.4). Moreover, this method avoids the need to identify spectral lines and to determine their centers to be compared with the laboratory wavelengths. Instead, it simply assumes that the spectral features in the observed star are (up to the measured Doppler shift) identical with those in a comparison star or a synthetic spectrum from a model atmosphere chosen as a template. The cross-correlation is usually performed numerically with digitalized observation, however, it is in principle analogy of the photoelectric measurement of radial velocities introduced by Griffin (1967) in which the measured spectrum of single or binary star (Griffin 1975) is matched against an appropriate diaphragm, e.g. a mask given by a template spectrum of a suitable comparison star.

The cross-correlation

$$F(v) \equiv \int I(x+v)J(x)dx \quad (1.11)$$

of the observed spectrum $I(x)$ with a properly chosen template spectrum $J(x)$ calculated in the logarithmic wavelength-scale x defined by (1.1) indicates by its extremes the velocity shifts v at which a similar contribution appears in the spectrum (cf. e.g. Simkin 1974,

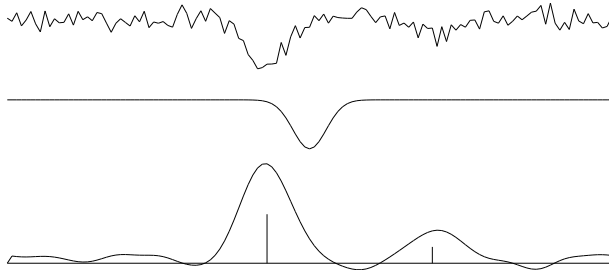


Figure 1.4: Example of cross-correlation – synthetic spectrum constructed as a superposition of lines of two components and a noise (the upper curve) correlated with an ideal line-profile (middle spectrum) gives a curve with amplitudes and positions of local maxima corresponding to the strengths and radial velocities of lines of the components (marked by vertical abscissae at the bottom curve), while the noise is smeared out by the integration.

Hill 1993).³ If the spectrum I is a superposition of spectra of two or more components, each of them contributes to F by its peak with maximum shifted for the instantaneous radial velocity of the component. The cross-correlation function F calculated for each exposure separately is thus fitted as a superposition of two or more Gaussian curves, which approximate the cross-correlations of individual components.⁴

An ideal template J should contain the same lines in the same ratios of their strengths as the spectrum of component to be measured. In practice an observed spectrum of a star of similar spectral type or a synthetic spectrum from a model-atmosphere are used. It should be noted that a misunderstanding is spread between many users who suppose that also the rotational broadening of the template J should be similar to that of the measured star and they even artificially broaden a slowly rotating or synthetic template J_0 taking $J = J_0 * R$.⁵ However, the cross-correlation with such J is identical with cross-correlation of I and J_0 additionally cross-correlated in with R (or equivalently convolved with its reverse). It means that the final cross-correlation is only smeared out, which makes its interpretation less precise.⁶

Some complication in the method may be due to side-peaks which arise in the cross-correlation function (CCF) from coincidence of lines in the observed spectrum with dif-

³In practice only the differences of the spectra from their continua are cross-correlated to subtract the large slowly varying contributions from the integral.

⁴Gaussian curves correspond to the thermal broadening of lines. However, the corresponding Maxwellian distribution is wider for light ions than for the heavier ones and it varies also with the temperature throughout the atmosphere. The Lorentzian wings and other individualities of different line profiles make the Gaussian approximation even more questionable. On the other hand, the turbulent broadening is often approximated by a Gaussian, the width of which equal for all particles is added (in squares – cf. Eq. (A.32)) to their thermal widths. Moreover, the profile of cross-correlation function is closer to Gaussian than the profiles of cross-correlated functions – cf. Eq. (A.34).

⁵It will be shown later that this commonly accepted procedure for “spinning” the profiles is a crude approximation inconsistent with the physics of stellar atmospheres.

⁶Spectra of stars with small rotational $v \sin i$ are thus preferable templates.

ferent lines in the template. These aliases are suppressed with increasing number of lines in the used spectral region (and they are not present at all for just one line). They are remote from the main peak of CCF if the lines are sparse in the region, but they may appear in the case of multiplets and blends of lines.

Experience with the method shows that the cross-correlation is not much sensitive with respect to the choice of the spectral type of the template spectrum. Nevertheless, the template spectrum should be known a priori. This can be quite difficult task to estimate for a faint companion.⁷ A partial aid in this respect may be the elegant option used by Bagnuolo et al. (1994) – to choose as the template a spectrum of the same binary taken near a conjunction, where both components have nearly the same radial velocity.

A generalization of this method is a two-dimensional cross-correlation

$$F(v_1, v_2) = \int I(x)[J_1(x - v_1) + J_2(x - v_2)]dx , \quad (1.12)$$

enabling one to choose templates corresponding to different spectral types for the primary and secondary component (cf. Zucker and Mazeh 1994, Zucker et al. 1995).

The same authors (Zucker and Mazeh 2006) tried to avoid the problem of finding a proper template in their modification of cross-correlation method which they designed for single-line binaries (and named TIRAVEL). Like in the disentangling, they use another exposure of the same star as a template and calculate a matrix $R(v_1, \dots, v_N)$ with components given by cross-correlations between all pairs of normalized exposures

$$R_{ij} = \int I(x - v_i, t_i)I(x - v_j, t_j)dx , \quad (1.13)$$

which is a function of radial-velocity shifts v_i of the star at individual exposures. The proper combination of these velocities giving the best alignment of all observed spectra is then indicated by maximum of the largest eigenvalue of R . The authors suggested a possibility to generalize their method for double-lined binaries using a combination with some method of decomposition, which would actually bring it closer to a method of disentangling. Zucker and Mazeh compared TIRAVEL with KOREL and they advertised alleged advantages of their method, which should consist in the fact that their velocities are free variables not bounded by an orbital motion. This claim reveals that they are not aware of KOREL's capabilities (for which mere radial velocities of SB1 are only an extremely trivial application). However, just in the case of perturbation by a third body, which they mentioned as an example of the need of free velocities, the possibility to converge parameters of both the close and the wide orbit is an advantage.

Even if the need of an external template would be avoided and coincidences between lines belonging to different components distinguished, there is still a disadvantage of

⁷As already mentioned, an attempt to overcome just this problem using a cross-correlation of spectra of the same binary obtained at different phases was one of the ideas from which the Fourier disentangling has arisen.

the cross-correlation technique caused by the fact that the cross-correlation profile is broadened due to widths of both the observed spectrum and the template (cf. Eq. (A.32)). This shortcoming of the cross-correlation method is well analyzed by Rucinski (2002), who developed a method of broadening function to overcome it.

1.3.2 Method of broadening function

In the method introduced by Rucinski (2002), the broadening function $B(x)$ is sought from observations to satisfy the relation

$$I = B * J \tag{1.14}$$

between the template J and the observed spectrum I . If the observed spectrum corresponds to a Doppler-shifted template or to a superposition of such shifted spectra for each component, then B is a shifted Dirac delta-function, or a sum of them. One or more components may also correspond to a broadened template spectrum (e.g. due to a rotation broadening). In favourable cases when lines of I are wide and lines of J are narrow, B will be a Doppler shifted broadening profile. For a given I and chosen J , Eq. (1.14) can be solved with respect to B using e.g. the SVD method. Position of peak of B gives again the information about the instantaneous Doppler-shift of the observed spectrum. The shape and especially the width of peak of B , which unlike F in Eq. (1.11) is not quadratic in the line profile, can yield also an information about the broadening of lines in I . An example of such a treatment of Schlesinger – Rossiter – Mc Laughling rotation effect from the profile of broadening function (cf. Albrecht et al. 2007).

In comparison with the method of cross-correlation function, the method of broadening function is a more direct way of interpreting the spectroscopic data, but the problem of the proper choice of the template persists in the later method and, it is at least equally important as in the former. A progress in detailed analysis of the observed broadening profile in this method can be implemented into disentangling and vice versa, but an important difference between these methods remains in the avoiding the need of template in disentangling.

1.4 Methods of decomposition of spectra

It is important to distinguish contributions of individual components of a multiple stellar system to its common spectrum not only to be able to measure the radial velocities and to solve for orbital parameters, but also to find the physical characteristics of atmospheres of the stars and to put them into context with their masses and evolutionary status.

An exceptional opportunity is yielded by eclipsing binaries for which spectrum of one component can be obtained during a total eclipse and the other spectrum can be found as its difference from spectrum obtained out of eclipse. However, for majority of stellar systems some more sophisticated methods must be used.

In principle, any method able to separate the spectra of components can be used in combination with any method for determination of radial velocities and orbital parameters as a part of the procedure of disentangling (i.e. as the right-hand green branch in the scheme of disentangling in Fig. 1 on p. 4). On the other hand, the versatility, preciseness and numerical efficiency of the chosen method of decomposition dominates the properties and applicability of the overall disentangling. It is thus worth to study different methods of the decomposition of spectra in details.

1.4.1 Direct subtraction

The most straightforward method of decomposition of spectra is the direct subtraction involved by Ferluga et al. (1991, 1997), in which two spectra I_a, I_b of a binary obtained at different phases (best of all at the opposite elongations, at extremes of radial velocities $v_{a,b}$ of both components) are used. If the spectra of individual components are J_1, J_2 , the relation

$$I_a(x) = J_1(x - v_{1a}) + J_2(x - v_{2a}) , \quad (1.15)$$

$$I_b(x) = J_1(x - v_{1b}) + J_2(x - v_{2b}) , \quad (1.16)$$

should be valid. From here we can calculate both spectra recurrently pixel by pixel

$$J_1(x) = J_1(x - v_{1a} + v_{1b} + v_{2a} - v_{2b}) - I_a(x + v_{1b} + v_{2a} - v_{2b}) + I_b(x + v_{1b}) , \quad (1.17)$$

$$J_2(x) = J_2(x - v_{1a} + v_{1b} + v_{2a} - v_{2b}) + I_a(x + v_{2a}) - I_b(x - v_{1a} + v_{1b} + v_{2a}) , \quad (1.18)$$

starting from a wavelength, where the spectra of both components can be approximated by continuum, and proceeding in positive or negative direction of the logarithmic wavelength variable x (depending on the sign of the expression $v_{1a} - v_{1b} - v_{2a} + v_{2b}$) toward groups of spectral lines.

This straightforward method clearly shows an obstacle, which is in principle a problem also for later more sophisticated methods. The region of values of x covered by each exposure contains information about spectra of individual components in regions shifted for $v_{1,2}$, so that the information on both spectra is available only in the overlap of both

regions. To be able to separate both spectra, one must add the missing information about the spectrum of the other component, usually the assumption that it is a pure continuum without any line. However, this can be a source of error, which may then spread also inside the region where the solution should be well determined.

The main disadvantage of this method is the fact, that owing to the recurrent procedure of solution the influence of random observational noise (which should be added on the right-hand sides of Eqs. (1.15) and (1.16)) is cumulative, so that after passing a group of spectral lines the solution can deflect from the correct value of the continuum. The influence of the noise can be reduced by averaging results of solutions obtained from a larger number of pairs of exposures. However, this suggests to develop a method searching *ab initio* for the best fit to a higher number of observed spectra, so that the solution $J_{1,2}$ of corresponding system of linear equations of type (1.15) would be overdetermined.

1.4.2 Iterative subtraction

Another similar method of decomposition of spectra based on an iterative procedure of subtraction has been introduced by Marchenko et al. (1998) as described by González and Levato (2006) who suggested to involve it in a kind of disentangling with radial velocities (and incorrectly referred to the full disentangling of orbital parameters by both Simon and Sturm 1994, and Hadrava 1995, as a decomposition only). This method overcomes the above mentioned disadvantage of Ferluga's method. It has been described for double-line binaries only, but it can easily be generalized to more than two components as follows.

Suppose we have N exposures taken at times $t_k|_{k=1}^N$ for which the radial velocities $v_j(t_k)$ of the components $j = 1, 2, \dots, n$ are known. According to Eq. (1.4)

$$I(x, t_k) = \sum_j I_j(x) * \delta(x - v_j(t_k)) . \quad (1.19)$$

To get estimate $I_j^{(i)}$ of spectrum I_j of the component j in the i -th step of the iteration (taking e.g. $I_j^{(0)} = 0$ as the initial approximation), we can average all observed spectra shifted to the rest wavelength-scale of the component j after subtracting the properly shifted estimates of spectra of other components according to their estimates in the previous step,

$$\begin{aligned} I_j^{(i+1)}(x) &= \frac{1}{N} \sum_{k=1}^N \left(I(x, t_k) * \delta(x + v_j(t_k)) - \sum_{l \neq j}^n I_l^{(i)}(x) * \delta(x - v_l(t_k) + v_j(t_k)) \right) \\ &= \frac{1}{N} \sum_{k=1}^N I(x, t_k) * \delta(x + v_j(t_k)) \\ &\quad - \sum_{l \neq j}^n I_l^{(i)}(x) * \left(\frac{1}{N} \sum_{k=1}^N \delta(x - v_l(t_k) + v_j(t_k)) \right) . \end{aligned} \quad (1.20)$$

Substituting here for $I(x, t_k)$ from Eq. (1.19), we get the difference between $I_j(x)$ and its estimate in the $i + 1$ -step

$$I_j^{(i+1)}(x) - I_j(x) = \sum_{l \neq j}^n (I_l(x) - I_l^{(i)}(x)) * \left(\frac{1}{N} \sum_{k=1}^N \delta(x - v_l(t_k) + v_j(t_k)) \right). \quad (1.21)$$

Fourier transform of this equation reads

$$\tilde{I}_j^{(i+1)}(y) - \tilde{I}_j(y) = \sum_{l \neq j}^n (\tilde{I}_l(y) - \tilde{I}_l^{(i)}(y)) \left(\frac{1}{N} \sum_{k=1}^N \exp(i(v_l(t_k) - v_j(t_k))y) \right). \quad (1.22)$$

It means that provided the radial velocities at individual exposures are so well randomly spaced over the orbital period that the complex exponentials in the last sum partly cancel each other for all Fourier modes y to a quantity smaller in absolute value smaller than 1 (it is again impossible for $y = 0$, but it can happen also for some harmonics of the orbital frequency), the method converges exponentially to the true solution of Eq. (1.19). As we shall see, the method is in practice equivalent with the subsequent method introduced by Bagnuolo and Gies much earlier and it cannot compete with the methods of disentangling. However, it may provide an alternative insight into these methods.

1.4.3 Method of tomographic separation

A method for decomposition of a larger number of observed spectra of a binary (with known radial velocities) was introduced already by Bagnuolo and Gies (1991). The averaging tendency of their method diminishes the observational noise in individual exposures.

This method is based on the mathematical equivalence of the task of decomposition with the problem of image reconstruction in tomography. The superposition of Doppler-shifted component spectra at different orbital phases can be treated as projection of two parallel linear objects (e.g. photographic spectrograms) viewed from different angles. Unlike the standard tomography, the line of a detector is not perpendicular to the direction of projection, but it remains parallel with the lines of component spectra (which differs by rescaling of each projection). Any standard numerical method of tomographic reconstruction should thus be able to calculate the distribution of intensities (or opacities) in this object of dimension $2 \times N$ from a higher number of exposures (each one consisting typically of N pixels) if a sufficient coverage of viewing angles / orbital phases is available – cf. Fig. 1.5.⁸

Bagnuolo and Gies chose the Iterative Least Square Technique – cf. Eq. (A.25). For a double-lined binary $N_2 = 2$. We suppose $K_2 > N_2$, $K_1 = N_1$ and approximate each bin

⁸The equivalence of both mathematical problems can be used also in the opposite direction, it means that numerical methods for spectra decomposition could be applied for computer tomography as well (cf. Hadrava 2001a).

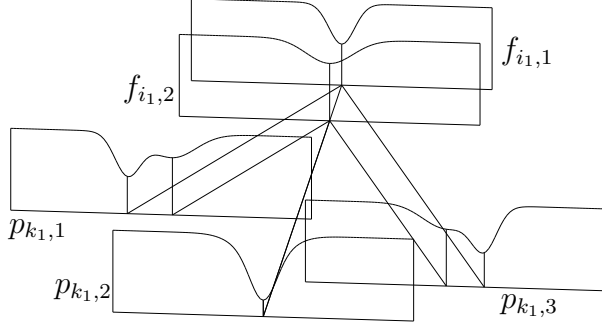


Figure 1.5: Principle of tomographic separation – projections of spectra of individual components (the two spectra in the back) into different directions correspond to different Doppler shifts in different phases (the three spectra in the foreground).

of a projection p_{k_1,k_2} as a superposition of both sources $f_{i_1,i_2}|_{i_2=1}^2$ Doppler shifted for the number of bins corresponding to the radial velocity $v_{i_2}(t_{k_2})$ of the component i_2 at the exposure time t_{k_2} (i.e. at the proper angle of projection in the view of tomography)

$$W_{k_1,k_2}^{i_1,i_2} = \delta_{k_1}^{i_1+v_{i_2}(t_{k_2})}. \quad (1.23)$$

Following Eq. (A.25) the correction of an estimate f_{j_1,j_2} reads

$$\Delta_{j_1,j_2} \simeq \frac{1}{K_2} \sum_{k_2} \left[p_{j_1+v_{j_2}(t_{k_2}),k_2} - \sum_{i_2} f_{j_1+v_{j_2}(t_{k_2})-v_{i_2}(t_{k_2}),i_2} \right]. \quad (1.24)$$

The basic idea of the equivalence of the decomposition with a tomographic reconstruction of projections of a rigidly rotating object does not allow a generalization to more components, with the exception of one, but an important case: it is the case when the spectrum of a third component does not move in radial velocities. This is the case of a background star in the view-field of the spectrograph, or presence of some interstellar lines, in some approximation also a third companion of the binary (if the amplitude of its radial velocities and velocities of the mass-centre of the close binary are small or their variations negligible during the observational run) or also a presence of telluric lines, if their seasonal variations of radial velocities may be neglected. Such a case of the third component has been really studied by Liu et al. (1997). In fact, despite the assumption of the rigid rotation was an inspiration for a development of the method, it is no more needed in the final formula (1.24), which is in fact equivalent to Eq. (1.20). The method is thus more general than its name suggests and it would be applicable to any multiple system as well.

The terminology of this method is misleading also from another point of view – it resembles a class of methods designed for the Doppler tomography, in particular tomographic reconstruction of circumstellar matter in interacting binaries (cf. e.g. Marsh and Horne 1988). The difference is that while the method by Bagnuolo and Gies aims at reconstruction of unknown spectra from their different superpositions (projections), the Doppler tomography reconstructs the distribution of emissivity in the velocity-space with

an emission line-profile postulated to be a δ -function in frequency. It would be desirable to decompose the intrinsic spectra (including their strength) for a field of sources distributed in the velocity-plane corrotating with the binary. However, such a problem does not have a unique solution; obviously, a rotating ring of δ -line emitters results at a double-peaked profile, which can also be produced by a static source with the same intrinsic line-profile. Nevertheless, a compromising problem could be solved if the solution would be constrained to some reasonably chosen subspaces of functions in both the spectral and velocity spaces.

The disadvantage of needing to know the radial velocities first is common for all mentioned methods of decomposition. However, complementing this approach with the method of cross-correlation, it is obvious that both the decomposition of the spectra and the measurement of radial velocities (and solution of orbital parameters) should be possible in an iterative process, without the ad hoc choice of the template spectrum. Such a task is solved by the methods of disentangling of spectra.

1.5 Method of wavelength-domain disentangling of spectra

The first method enabling simultaneous decomposition of the spectra of binaries and measurement of their radial velocities, or actually directly the solution of orbital parameters was published by Simon and Sturm (1994).⁹

The decomposition of the spectra is solved by Simon and Sturm (similarly as in the methods by Ferluga or Bagnuolo and Gies) directly for $2M$ values of spectral fluxes \mathbf{I}_A and \mathbf{I}_B of components A and B at individual values of the independent variable x (here M corresponds to the number of pixels in the typical exposure which is typically of the order 10^3). A set of $N \times M$ linear equations

$$\begin{pmatrix} \mathbf{M}_{A1} & \mathbf{M}_{B1} \\ & \dots \\ \mathbf{M}_{AN} & \mathbf{M}_{BN} \end{pmatrix} \begin{pmatrix} \mathbf{I}_A \\ \mathbf{I}_B \end{pmatrix} = \begin{pmatrix} \mathbf{I}(t_1) \\ \dots \\ \mathbf{I}(t_N) \end{pmatrix}, \quad (1.25)$$

is obtained for these unknown values, where N is the number of exposures (it must be $N \geq 2$). There are N subvectors $\mathbf{I}(t_l)$ of dimension M with spectra observed at times $t_l|_{l=1}^N$ of exposures on the right-hand side of this equation. In the simplest form, the submatrices

$$\mathbf{M}_{jl} = \begin{pmatrix} \overbrace{0 \quad \dots \quad 1}^{v_j(t_l)} & \dots \\ 0 & & 1 & \\ & \dots & & \\ \dots & 0 & \dots & 1 \\ & \dots & & \\ & \dots & & 0 \end{pmatrix} \quad (1.26)$$

of dimension $M \times M$ on the left-hand side have the only nonzero elements equal to 1 shifted from the main diagonal for a number of pixels corresponding to the values $v_j(t_l)$ of Doppler shift of component $j|_{j=A}^B$ at time t_l . The form of the matrices may be more tricky to include also the interpolation from input data which would not be sampled in the same grid points. Another option is to enlarge the matrices for additional $\max(v_j(t_l))$ columns on each side and correspondingly to enlarge the vectors $\mathbf{I}_{A,B}$ for wavelengths, which appear in the windows $\mathbf{I}(t_j)$ in some exposures only. This enlarging of the window may help to abandon the edge-errors of the decomposition in the cases when it is impossible to prevent all lines from escaping from the window by proper choice of its limits. However, these regions behind the edges will be less and less overdetermined and hence the noise may increase therei, like in the method of the direct subtraction.

⁹They also introduced for their method the name ‘disentangling’, which is used here to denote the problem in this complexity.

Simon and Sturm solved the set of equations which has a sparse matrix but of very high dimension using the method of ‘singular value decomposition’. This method has been applied on real data in several studies (e.g. Sturm and Simon 1994, or Simon et al. 1994). It could be mentioned that the method was tested also by Hynes and Maxted (1998) using some simulated data.

It should be noted that Simon and Sturm introduced their method in this simple form for two components only. Obviously, it is straightforward to generalize it for more components by increasing the number of the columns with the submatrices. The authors mentioned that they give the simplest unit off-diagonal form of the submatrices, which requires to rebin all input data into the same equidistant scale, but they could be constructed in a more complicated form to interpolate directly in an arbitrary sampling. Their form of the submatrices implies also that the Doppler shifts must be rounded to an integer multiple of the sampling step. As I shall show later, it is also possible to increase the resolution in radial velocities below the bin size by an appropriate construction of a three-(off-)diagonal submatrix.

Despite of the fact that the decomposition of the spectra is the more difficult part of the disentangling, including the solution of orbital parameters into the same procedure represents an essential qualitative advance in the interpretation of the stellar spectra. An ideal procedure of any interpretation would be to fit the observational data by a complete theoretical model and to estimate, how far the conclusions of the study are determined by the original observations. If this task is split into subsequent steps like the determination of radial velocities in individual exposures first and the solution of radial-velocity curves only after, the information about the decisive power of the source data is partly lost in the questionable reliability of the intermediate results. This is a reason to prefer the direct solution of orbital parameters instead of disentangling of component spectra together with their radial velocities¹⁰ and the same strategy leads us to consider a further generalization of the method of disentangling to include simultaneously some other effects, like the line-profile variability. At the same time, the user must be aware that the choice of a particular model to fit the data may be biased and even good results do not exclude that some other model may better explain the same data or data enriched by some additional observations.

¹⁰Such an option may be preferable if the spectra contain a component which need not follow any orbital motion, like an absorption in gaseous streams projected on photospheres of components in interacting binaries.

1.6 Fourier disentangling and its generalizations

Unlike the approach by Simon and Sturm, which is based on the decomposition of spectra in the wavelength domain, KOREL uses the least square fit of Fourier transforms of observed spectra (Hadrava 1995, cf. Section 1.6.1), which makes the solution numerically easier and which thus enables further generalizations (see e.g. Hadrava 1997, 2004a and Sections 1.6.3 and 1.6.5). The mathematical basis of the present method is analogous to the cross-correlation technique, however, the basic difference from the standard cross-correlation (e.g. Hill 1993) or its two-dimensional generalization (Zucker and Mazeh 1994) is that in KOREL all spectra at different phases of the same variable star are mutually compared and decomposed instead of performing cross-correlation of each spectrum of the variable separately with an ad hoc chosen standard. Numerous applications of this method to real data have been reviewed by Holmgren (2004).

1.6.1 Principle of Fourier disentangling

We shall return now to details of the Fourier disentangling outlined already in Section 1.1. Before explaining the procedure of solution of Eqs. (1.4) or (1.5), let us generalize them for purposes of later development of the method. In view of the possibility to involve a broadening of line-profiles similarly as the Doppler shifts by another convolution with a corresponding broadening profile (cf. Eq. (1.14)), we can generalize Eq. (1.4) to

$$I(x, t) = \sum_{j=1}^n I_j(x) * \Delta_j(x, t, p) , \quad (1.27)$$

and its Fourier transform to

$$\tilde{I}(y, t) = \sum_{j=1}^n \tilde{I}_j(y) \tilde{\Delta}_j(y, t, p) , \quad (1.28)$$

where Δ_j are some general broadening functions, which may involve now not only the Doppler shifts, but possibly also some line-profile broadenings at the time t ; $\tilde{\Delta}_j$ are their Fourier transforms. These functions depend on some parameters p characterizing either the orbital motions of the components or physical and geometric conditions of formation of their spectra.

The principle of disentangling consists in minimization of the sum of integrated squares of differences between the observed and model spectra (on the left and right hand sides of Eq. (1.27), respectively)

$$0 = \delta \sum_{l=1}^N \int \left| I(x, t_l) - \sum_{j=1}^n I_j(x) * \Delta_j(x, t_l, p) \right|^2 dx , \quad (1.29)$$

which is supposed to be due to observational noise in $I(x, t)$. This expression implicitly assumes, that the noise is the same for all wavelengths. Only limited spectral regions are available in practice, which means that outside the corresponding range of x we take the spectra with zero weight. The minimization is performed with respect to the component spectra $I_j(x)$ (which gives the decomposition of the spectra) as well as to the orbital parameters (corresponding to the solution of radial-velocity curves with implicitly involved radial velocity measurements) or other free parameters p .

According to the Parseval theorem (A.5), the condition (1.29) can be equivalently rewritten as minimization (i.e. zero variation) of sum of integrals of the Fourier transforms

$$0 = \delta \sum_{l=1}^N \int \left| \tilde{I}(y, t_l) - \sum_{j=1}^n \tilde{I}_j(y) \tilde{\Delta}_j(y, t_l, p) \right|^2 dy . \quad (1.30)$$

This form of the condition assumes implicitly, that the noise is white, which need not be always the case, as we shall discuss later. It can thus be better to involve some weights $w_l(y)$ of individual Fourier modes and to write the condition in the form

$$0 = \delta S , \quad (1.31)$$

where

$$S = \sum_{l=1}^N \int \left| \tilde{I}(y, t_l) - \sum_{j=1}^n \tilde{I}_j(y) \tilde{\Delta}_j(y, t_l, p) \right|^2 w_l(y) dy . \quad (1.32)$$

The equation for decomposition of spectra can be obtained by varying S with respect to individual Fourier modes,¹¹

$$\begin{aligned} 0 &= \frac{\partial S}{\partial \tilde{I}_m^*(y)} = - \sum_{l=1}^N \left[\tilde{I}(y, t_l) - \sum_{j=1}^n \tilde{I}_j(y) \tilde{\Delta}_j(y, t_l, p) \right] \tilde{\Delta}_m^*(y, t_l, p) w_l(y) = \\ &= \sum_{j=1}^n \left[\sum_{l=1}^N \tilde{\Delta}_j(y, t_l, p) \tilde{\Delta}_m^*(y, t_l, p) w_l(y) \right] \tilde{I}_j(y) - \sum_{l=1}^N \tilde{I}(y, t_l) \tilde{\Delta}_m^*(y, t_l, p) w_l(y) \end{aligned} \quad (1.33)$$

which is obviously a set of n linear equations for each Fourier mode separately.

The solution is similar to quantum mechanics, where any linear operator can be equivalently written in different representations, however, it is easier to calculate its functions and in particular its inversion in a reducible representation. This is the basic trick which makes the Fourier disentangling more versatile compared to the wavelength domain disentangling, despite in principle both methods are equivalent and their general features,

¹¹Because \tilde{I} are complex values, the partial derivatives of S must be calculated either independently with respect to their real and imaginary parts, or with respect to \tilde{I} and its complex conjugate as independent variables.

which are easier to understand in one representation are in fact valid for the other as well.¹²

Regarding that $I_j(x)$ are real values, the Fourier transform \tilde{I}_j must satisfy

$$\tilde{I}_j(-y) = \tilde{I}_j^*(y) , \quad (1.34)$$

i.e. its real part must be symmetric and the imaginary part antisymmetric. It is thus sufficient to solve $n/2$ independent complex linear equations. Similarly, the matrix $a_{mj} \equiv \sum_l \tilde{\Delta}_j(y, t_l, p) \tilde{\Delta}_m^*(y, t_l, p) w_l(y)$ to be inverted for the solution is Hermitean, so that only one triangular part of it must be computed according to the definition and the other part is given by the symmetry.

To optimize the solution with respect to the parameters p we can use the conditions

$$0 = \frac{\partial S}{\partial p} = -2\Re \sum_{l=1}^N \int \left[\tilde{I}(y, t_l) - \sum_{j=1}^n \tilde{I}_j(y) \tilde{\Delta}_j(y, t_l, p) \right] \sum_{m=1}^n \tilde{I}_m^*(y) \frac{\partial \tilde{\Delta}_m^*(y, t_l, p)}{\partial p} w_l(y) dy . \quad (1.35)$$

However, the dependence of $\tilde{\Delta}_j$ on p can be generally quite complicated and consequently also the solution of these equations may be difficult. It can thus be easier to minimize directly the expression for S in the form (1.32) using some numerical method of optimization, like the simplex method.

Let us note that despite the determination of radial velocities and subsequent solution of radial-velocity curve is an obsolete procedure compared to the disentangling of spectra, it may be still useful to determine radial velocities for individual exposures first to enable their combination with older data from literature or with solution of light-curves. Having already disentangled a set of spectra, it is possible to measure radial velocities of the component stars in each of them by fitting the spectrum as a superposition of the disentangled spectra Doppler-shifted for velocities independent of the found orbital parameters.

As noted by D. Holmgren, it is interesting to mention that the Fourier method of spectra decomposition was in a way anticipated by the analysis of line-profile variability in the form of traveling features in the spectra of ζ Oph by Walker et al. (1979).

1.6.2 Simple Fourier disentangling

Let us illustrate the Fourier disentangling first in the simple case, which is equivalent to the above explained method by Simon and Sturm (cf. Section 1.5), with the only

¹²It is obvious that for the special case $n = 2$, Eqs. (1.4) or (1.5) are equivalent with Eq. (1.25). Consequently, it is incorrect, what Simon and Sturm (1994, p. 291) claim, that unlike the problem of tomography, which is analytical by its nature, the decomposition or disentangling is the algebraic one. Both these problems, as well as others related with them, can be formulated analytically and solved algebraically in a chosen numerical representation. The generalizations of disentangling given below could be, in principle, done also in the wavelength domain as it was done in the pioneering work by Simon and Sturm. However, the numerical solution would be then more difficult.

generalization that the observed system need not be a binary only, but it may consist of n stars. Then Δ -functions corresponding to the pure Doppler shifts are given by

$$\Delta_j(x, t, p) = \delta(x - v_j(t, p)) , \quad (1.36)$$

their Fourier transforms are

$$\tilde{\Delta}_j(y, t, p) = \exp(iy v_j(t, p)) , \quad (1.37)$$

and consequently (if we skip the weights $w_l(y)$ for simplicity) Eq. (1.33) reads

$$\sum_{j=1}^n \left[\sum_{l=1}^N \exp(iy(v_j(t_l, p) - v_m(t_l, p))) \right] \tilde{I}_j(y) = \sum_{l=1}^N \exp(-iy v_m(t_l, p)) \tilde{I}(y, t_l) . \quad (1.38)$$

This set of equations can be solved with respect to $\tilde{I}_j(y)$ whenever the matrix (with indices j, m) on the left-hand side is non-singular.

It is obvious that the singularity occurs always for $y = 0$ (which can be seen also in Eq. (1.5)), when this equation reduces for all m to a single condition

$$\sum_{j=1}^n \tilde{I}_j(0) = \frac{1}{N} \sum_{l=1}^N \tilde{I}(0, t_l) \quad (1.39)$$

for the sum of mean values of the component spectra to give the mean value of the observed spectra. It means, that the continua cannot be directly decomposed, because they are not influenced by the Doppler shifts. An indirect method of distinguishing the contributions to the continuum is described in Section 1.6.4. This problem will be discussed in detail in Section 1.6.10. It can happen also for non-zero Fourier modes that the matrix is nearly singular and the solution is thus unstable. This danger is higher for low modes, for which the Doppler effect is smaller. These modes can be more influenced by errors in rectification of spectra. This is why it may be better to filter them out using some weights $w_l(y)$ as additional multipliers in the integrals in expression (1.32). These multipliers will not influence the decomposed spectra directly by the amplitudes and phases of individual Fourier modes but through the optimal values of the parameters p . It is possible in KOREL to cut out a chosen number of lowest modes.¹³

As mentioned in the previous Section, limited ranges with a finite sampling are used in practice both in the wavelength domain as well as in the domain of the Fourier transforms of spectra. The highest efficiency of numerical calculation is achieved if the numbers of

¹³Iljić et al. (2000) advocate a filtering of high frequency noise from spectra before the disentangling. It would be possible to involve the filtering directly into the procedure of disentangling, if such a need will be confirmed. The present version of KOREL does not allow it not to complicate much its use. Some filtering of high frequencies is performed already by the interpolation of the original data into the chosen scale of x .

bins in both representations are comparable. The Fourier transform between these limited sets of discretized data points assumes a periodic repeating. It means that a spectral line which disappears at some phase behind one edge of the spectral region to be decomposed is expected to appear at the other. Because this will not generally happen (unless by chance a similar line exists at the other edge), solution of decomposition cannot fit at the edges all observed spectra with and without the line. This leads to errors propagating from edges toward the middle of the decomposed range, as described by Ilić et al. (2000). To prevent these errors the spectral regions chosen for the disentangling should have continua¹⁴ without spectral lines at both edges of the decomposed spectral range, best of all wider than the expected amplitude of radial velocities of the components. To facilitate the choice of convenient spectral range code PREKOR has been written, which interpolates from the data-files with individual exposures into chosen regions with proper discretization and displays the result to enable a visual check of the input data for KOREL. It may be difficult to satisfy the demand for pure continua at edges of the region when disentangling is applied to late-type stars. In such a case the edge defects can be partly suppressed by the so called tapering of the signal towards the edges (or the hemming of signal window), i.e. a smooth suppressing the signal of source data in narrow strips on both edges towards the continuum, as it is recommended also in the technique of cross-correlation. This trick is in fact similar to the choice of slightly higher dimension of decomposed vectors $\mathbf{I}_{A,B}$ on the left-hand side of Eq. (1.25) of the method by Simon and Sturm than is the dimension of the source data $\mathbf{I}(t_l)$ on the right-hand side.

1.6.3 Line-strength variations and removal of telluric lines

The simplest generalization of the disentangling is to abandon the assumption of constant component spectra and to admit a change of strength of lines of some component. The original motivation for this step was the experience that in some binaries errors of radial velocities increased significantly close to conjunctions where an eclipse could be expected. If the contribution of one eclipsed star is missing in the spectrum of the whole system, the spectra of the remaining are more pronounced and their sum cannot be fitted so well as a superposition of lines with the same depths as out of the eclipse.

The effect of eclipse may be even more complex e.g. due to the Schlesinger – Rossiter – McLaughlin rotation effect, however variations of line strengths are observed also as the so called Struve – Sahade effect (cf. Stickland 1997), they are characteristic for circumstellar lines or telluric lines etc. The calculation of the line-strength factors may also partly compensate some instrumental and data-processing imperfections like incorrect flatfielding or rectification.

Let us thus generalize Eqs. (1.36) and (1.37) by involving multiplicative line-strength

¹⁴Naturally the continua on both edges of each spectral region should have the same level to prevent also a discontinuity in jump between the edges of decomposed spectra. This can be ensured by the rectification of input spectra to their continua.

factors $s_j(t)$, i.e.

$$\Delta_j(x, t, p) = s_j(t) \delta(x - v_j(t, p)) , \quad (1.40)$$

the Fourier transforms of which read

$$\tilde{\Delta}_j(y, t, p) = s_j(t) \exp(iy v_j(t, p)) . \quad (1.41)$$

In this case Eq. (1.33) gets slightly more complicated form compared to (1.38), namely

$$\begin{aligned} \sum_{j=1}^n \left[\sum_{l=1}^N w_{l,X}(y) s_{jl} s_{ml} \exp(iy(v_j(t_l, p) - v_m(t_l, p))) \right] \tilde{I}_{X,j}(y) &= \\ = \sum_{l=1}^N w_{l,X}(y) s_{ml} \exp(-iy v_m(t_l, p)) \tilde{I}_X(y, t_l) . \end{aligned} \quad (1.42)$$

Here $s_{jl} \equiv s_j(t_l)$ and the subscript X refers to different regions of the observed spectra, each one being characterized by its initial wavelength x and its dispersion (in the value of radial velocity per one bin of the sampling in x). The weights $w_{l,X}(y)$ could be, in principle, different for each Fourier mode y in each spectral region X of the exposure l . However, in the present version of KOREL, we choose¹⁵

$$w_{l,X}(y) = w_{l,X} w(y) . \quad (1.43)$$

The weight $w_{l,X}$ of each exposure can be chosen, e.g., in dependence on the number of photon counts. The spectral filter $w(y)$ enables to cut out the lowest Fourier modes, as mentioned at the note ¹³ on page 28.

Following (1.41), S given by (1.32) is bilinear also in coefficients s_{jl} . Hence, varying with respect to s_{ml} , we get from Eq. (1.35) for each chosen exposure l the following set of linear equations

$$\begin{aligned} \sum_{j=1}^n \Re \left[\sum_X \int w_{l,X}(y) \tilde{I}_{X,j}(y) \tilde{I}_{X,m}^*(y) \exp(iy(v_j(t_l, p) - v_m(t_l, p))) dy \right] s_{jl} &= \\ = \Re \sum_X \int w_{l,X}(y) \tilde{I}_X(y, t_l) \tilde{I}_{X,m}^*(y) \exp(-iy v_m(t_l, p)) dy \end{aligned} \quad (1.44)$$

for these coefficients corresponding to different components. It is obvious from Eqs. (1.28) and (1.41) that for each component its spectrum $\tilde{I}_j(y)$ and strengths s_{jl} are defined by the observations up to a reciprocal multiplier. This must be fixed by a normalization condition.

¹⁵The weights $w_{l,X}$ are part of input data for KOREL. They can be chosen before running PREKOR and altered for selection of different regions X if these are merged from different runs of PREKOR. The filter $w(y)$ is taken as the same function of the order of Fourier harmonic for all l, X which means that its scale in wavelengths of the original spectra is dependent on sampling in X .

If strengths of some components are fixed, their terms must be transferred from the left- to the right-hand side of this equation. Because the coefficients s_{jl} are generally still quite numerous (but less in number than the Fourier modes of the component spectra), it is advantageous to solve for them directly from equations (1.44) before optimizing S with respect to either $v_j(t_l)$ or p , in which it is non-linear.

It is important to hold in mind that the solutions of orbital elements (or individual independent radial velocities), the decomposition of the spectrum and the solution of component strengths are inter-related and their self-consistent solution should be found. To find this solution, an iterative procedure is used if all these kinds of unknowns are allowed to converge. However, there is no guaranty that this scheme will converge from every arbitrarily chosen initial condition. Instead, it can achieve some false local minimum by suppressing lines in exposures for which the true radial velocities differ from the instantaneous approximation or orbital parameters. It is thus often more efficient to approximate the solution of spectra and orbital parameters with fixed strengths (either found in some other spectral region, where lines of given components are better pronounced, or simply let them equal to one) first and to allow them to converge for a final tuning of the solution only.

The option of line strength solution enables a decomposition of the telluric lines (or, in principle, also some interstellar lines) from the observed spectra. Exactly speaking, the telluric component of the spectrum is not additive, but multiplicative, because the observed spectrum

$$I_{obs}(x, t) = \exp(-\tau(x, t))I_0(x, t) \quad (1.45)$$

is proportional to the true composed spectrum I_0 of the studied stellar system as seen outside the Earth's atmosphere. However, this formula can be approximated as

$$I_{obs}(x, t) = I_0(x, t) + I_{tell}(x, t) , \quad (1.46)$$

where telluric spectrum

$$I_{tell}(x, t) = (e^{-\tau(x, t)} - 1)I_0(x, t) \simeq -\tau(x, t)I_0(x, t) \quad (1.47)$$

is a negative contribution in lines with no continuum.¹⁶ The optical depth τ and hence also strength of telluric lines is very sensitive to the air-mass and humidity at each exposure. Because usually we are not interested in the true telluric spectrum $\tau(x, t)$ but only in how to eliminate its influence, we can decompose its lines traveling with the annual motion of the Earth as they are imprinted on the mean $I_0(x)$. A small discrepancy may arise only with telluric lines falling on steep slopes of line profiles in $I_0(x)$, the strength of which in ratio to the strengths of lines falling to continuum of $I_0(x)$ can differ in each exposure depending on the instantaneous radial velocities.

¹⁶The small telluric absorption in continuum is eliminated by the rectification of the observed spectra.

1.6.4 Line photometry

Taking into account the connection between formation of continuum and spectral lines in stellar atmospheres, the above described method for calculation of line-strength variations yields a possibility to find differential magnitude changes between the components and also to determine the ratio of component continua in the case that the intensity variations are caused by some overall darkening of a component e.g. by an eclipse. Let in the ‘normal’ state of a binary (i.e. out of eclipse) the intensities $I_{1,2}$ of components continua be normalized

$$I_1 + I_2 = 1 . \quad (1.48)$$

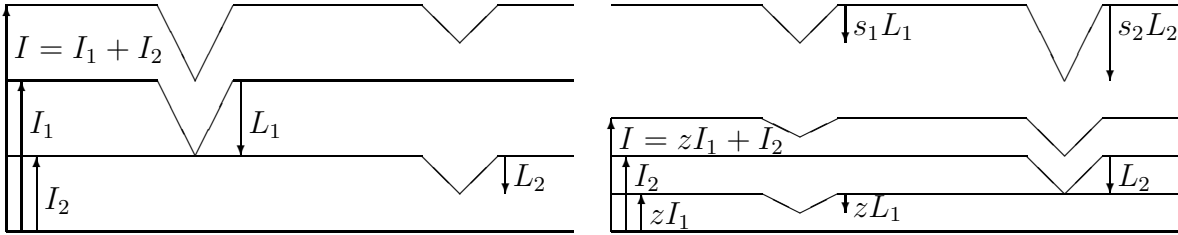


Figure 1.6: Continuum and line strengths of uneclipsed components (left) and in the primary eclipse (right).

The line depths $L_{1,2}$ of the components found by solution of Eq. (1.42) are expressed in units of this common continuum with respect to which the input spectra were rectified. If in another exposure the spectrum of component ‘1’ is decreased by factor $z \times$ (see Fig. 1.6), then the decomposed line depths of both components referred to the instantaneous common continuum will be changed by factors $s_{1,2}$ to values

$$s_1 L_1 = \frac{z_{lin} L_1}{z_{cont} I_1 + I_2} \quad (1.49)$$

$$s_2 L_2 = \frac{L_2}{z_{cont} I_1 + I_2} . \quad (1.50)$$

The factor z_{lin} can thus be simply expressed as

$$z_{lin} = \frac{s_1}{s_2} , \quad (1.51)$$

and assuming that the factor z in continuum is the same, $z_{cont} \equiv z_{lin}$, the ratio of continua intensities can be also found as

$$\frac{I_1}{I_2} = \frac{1 - s_2}{s_1 - 1} . \quad (1.52)$$

Obviously, if $z < 1$, then $s_1 < 1$ and $s_2 > 1$. This behavior can help to distinguish the variations caused by the ‘geometrical’ reasons (or their equivalent) from intrinsic variations of line intensities of a component or from the observational noise.

In the usual case of N exposures, the factors $z_l|_{l=1}^N$ of the darkenings of the component ‘1’ can be calculated independently for each exposure from s_{jl} according to Eq. (1.51). The ratio of continua intensities can be then obtained by least square fit of Eqs. (1.49) and (1.50) e.g. in logarithmic (i.e. magnitude) scale, i.e. by solving the condition

$$0 = \delta \sum_l [\ln s_{2l} + \ln(1 + I_1(z_l - 1))]^2 \quad (1.53)$$

for the variation δI_1 .

The applicability of this simple estimate of ratio of continua from line photometry is limited by the above mentioned assumption that the change of intensity is the same for the line and the continuum and certainly also by assumption that only two components are present as well as that there are no intrinsic changes of line profile shapes. Practical experience indicated that this is not exactly true even for eclipsing binaries, not to speak about stars where intrinsic line-profile variability can be expected due to ellipticity, radial or non-radial pulsations, spots or reflection. The reason can be simply understood in terms of limb-darkening variations within the line-profile. If the limb darkening is different in line and in continuum, the portions z of eclipsed light in numerator and denominator in Eq. (1.49) are different and cannot be solved together with $I_{1,2}$ from $s_{1,2}$, unless their relation is known from theory. On the other hand, fitting of $s_{1,2}$ by a more detailed model of eclipse light-curves in each x can reveal the limb-darkening variations within the line and thus yield information about the structure of atmosphere of the eclipsed component.

As shown in a preliminary study of this problem (Hadrava and Kubát, 2003), the variations of line profile across the stellar disk are generally very complex, so that even the often used expression of rotational broadening as a convolution with some rotational profile is in fact wrong. However, some relatively good approximations can be developed from the theory of stellar atmospheres, which will simplify the task to a solvable and quite powerful method.

If source-function in a plane-parallel atmosphere can be expanded into a Taylor-series in monochromatic optical depth

$$S(x, \tau) = \sum_k \frac{1}{k!} S_k(x) \tau^k, \quad (1.54)$$

the surface intensity is polynomial in directional cosine μ with coefficients S_k ,

$$I(x, \mu)|_{\tau=0} = \sum_k S_k(x) \mu^k. \quad (1.55)$$

In the Milne-Eddington approximation these sums reduce to the first two terms, so that the distribution of intensity over the visible stellar disk

$$I(x, \mu)|_{\tau=0} = S_0(x) + S_1 \mu = I(x, 1)|_{\tau=0} (1 - u + u\mu) \quad (1.56)$$

corresponds to linear limb darkening

$$u = \frac{S_1}{S_0 + S_1} , \quad (1.57)$$

which is according the theory $u = \frac{3}{5}$ for the light integrated in frequencies and according to solutions of observed light-curves around $u \simeq 0.3$ for the visible light in wide frequency bands, i.e. in continuum.

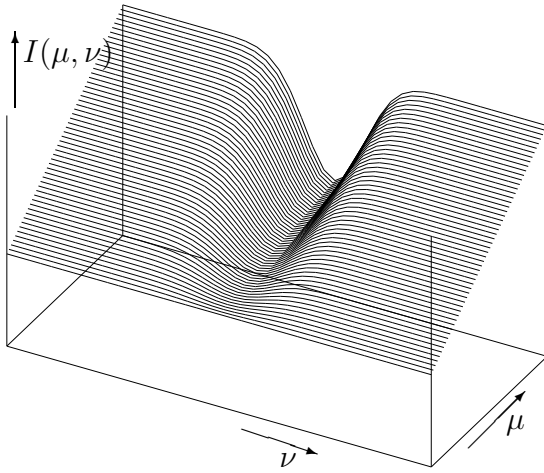


Figure 1.7: Schematic dependence of limb darkening across line-profile of an absorption line. Intensity is low on edge of stellar disk ($\mu = 0$) both in continuum and the line, but it is more brightened toward the disk centre ($\mu = 1$) in continuum than in the line, because the radially escaping photons in continuum originate in deeper and hotter layers of the atmosphere. The central parts thus contribute to the formation of spectral lines with increasing weight.

Suppose that in all geometric depths (radii of the star r) the monochromatic opacity across a line-profile is proportional to the opacity in continuum with the same line-profile function ϕ dependent on the frequency x only.¹⁷ Then also the monochromatic optical depth τ is proportional to the optical depth in continuum,

$$\tau(x, r) = [1 + \phi(x)]\tau_{cont}(r) . \quad (1.58)$$

If conditions of LTE are satisfied for studied lines, S is a smooth (Planckian) function of x , so that its change within the line profile can be neglected and its slope in monochromatic optical depth varies only due to the opacity profile, $S_1(x)[1 + \phi(x)] \simeq S_{1,cont}$. The linear limb-darkening is thus decreasing toward the center of line

$$I(x, \mu)|_{\tau=0} = S_{0,cont} + S_{1,cont}[1 + \phi(x)]^{-1}\mu , \quad (1.59)$$

and the line-contribution to the spectrum

$$[I(x, \mu) - I_{cont}(\mu)]_{\tau=0} = -S_{1,cont} \frac{\phi(x)}{1 + \phi(x)} \mu , \quad (1.60)$$

¹⁷This is not true generally. However, we can take the assumption of separability in variables r and x as the first approximation at least in a small region where the core of the line is formed.

which is negative, has distribution over the stellar disk corresponding to limb-darkening

$$u_{lin} = 1. \quad (1.61)$$

It means that at initial phases of an eclipse when only a part of disk edge is hidden, the light missing in line represents larger portion of the overall flux in that frequency than the light missing in the continuum ($z_{lin} < z_{cont}$), so that in some cases line-strengths of both components can be enhanced. The z -factors from Eqs. (1.49) and (1.50) for an eclipse must be thus modelled simultaneously for the continuum and lines with their corresponding limb-darkenings. The geometric parameters of the eclipse can be converged to fit the observed line-strength variations like in the standard procedure of light-curve solution. However, despite such a procedure is a significant improvement compared to the standard methods, it is still limited by several assumptions, which are never exactly satisfied.

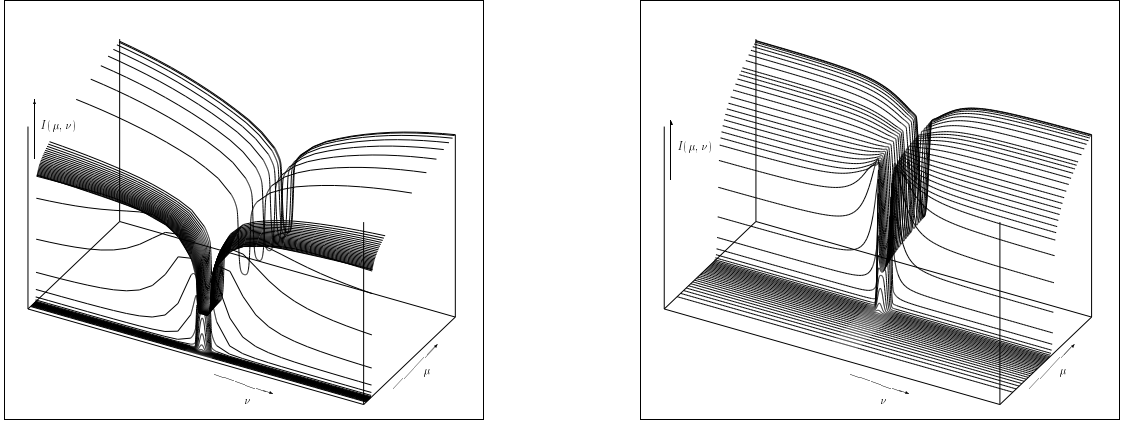


Figure 1.8: Limb darkening across the H α line-profile of hydrogen-helium non-LTE spherical model atmospheres with (left:) $T_{\text{eff}} = 15000 \text{ K}$, $\log g = 4.5$ ($L = 1.7 \cdot 10^2 L_{\odot}$, $M = 4.3 M_{\odot}$, $R = 1.9 R_{\odot}$) and (right:) $T_{\text{eff}} = 15000 \text{ K}$, $\log g = 2.0$ ($L = 5 \cdot 10^5 L_{\odot}$, $M = 4 M_{\odot}$, $R = 33.1 R_{\odot}$).

1.6.5 Disentangling with intrinsic line-profile variations

In view of the fact that components of binaries are often subjected to different kinds of variations and asymmetries (already mentioned ellipticity, reflection, spots, radial as well as nonradial pulsations), which are manifested as line-profile variations, the method of disentangling needs a further generalization. If some of these effects becomes non-

negligible, the basic equation (1.4) must be replaced by a more detailed expression

$$I(x, t) = \sum_{j=1}^n \int_s \mu I_j(x, s, \mu, t) * \delta(x - v_j(s, t)) d^2s, \quad (1.62)$$

for the spectral flux as an integral of the local monochromatic intensities over the visible parts of surfaces s of individual components j , each one Doppler shifted according to the local radial velocity, which can reflect now not only the orbital motion, but also rotation and pulsation of the stellar atmosphere. It should be noted that this expression is already simplified substantially, because it neglects the changes of radial velocity along the line of sight. This model of the atmosphere moving as a whole is commonly used in studies of non-radial stellar pulsations (cf., e.g., Townsend 1997), however, observations of different Doppler shifts of lines with different excitation potentials in Cepheids (e.g. Butler 1993) reveal, that it is not exactly the truth. A similar problem may arise in the case of stellar winds or disk-like envelopes, etc.

The unknown functions I_j depend now on a larger number of variables than the observed spectra on the left-hand side, equally as the velocities v_j . Consequently these functions cannot be reconstructed from the observed spectra without some additional conditions like it was in the previous case of surface homogeneity. Such a condition can be based either on some geometric or physical assumption. For a suitable choice of some sets of functions for I_j and v_j , their free parameters can be adjusted to fit the observed spectra. However, it must not be forgotten that the solution is model dependent and that in principle it cannot be excluded that some other model may fit the data equally well or even better.

Quite generally (c.f. Hadrava 1997) the local intensity can be expressed as a linear combination of a few spectral functions I_j^k

$$I_j(x, s, \mu, t) = \sum_k f_j^k(s, \mu, t) I_j^k(x) \quad (1.63)$$

with coefficients f_j^k whose dependence on the position on the star-surface s , directional cosine μ and time t can be modelled up to a few free parameters. Substituting this into Eq. (1.62) we arrive at equation

$$I(x, t) = \sum_{j,k} I_j^k(x) * \Delta_j^k(x, t, p), \quad (1.64)$$

which is formally identical with (1.27), apart of the fact that each component j can be now characterized by several spectra $I_j^k(x)$ (e.g. corresponding to different terms in the expression (1.55) for the limb darkening, or to spectra inside and outside a spot etc.) with different spectral broadenings

$$\Delta_j^k(x, t, p) = \int_s \mu f_j^k(s, \mu, t) \delta(x - v_j(s, t)) d^2s. \quad (1.65)$$

Differences in these broadenings can ensure that the corresponding spectral functions can be decomposed from the observations using the general procedure described in Section 1.6.1.

1.6.6 Broadening by pulsations

One of the simplest generalizations of disentangling for a case of intrinsic line-profile variations, which was outlined in the Section 1.6.5, is the problem of pulsating stars. Suppose first, that the atmosphere of a spherical star moves as a whole radially (with respect to its center) with instantaneous velocity $v_p(t)$. In agreement with conclusion (1.61) let us simplify the sum (1.63) to a single term linear in the directional cosine $\mu = \cos \vartheta$, which is a function of the projected distance $r = R \sin \vartheta$ from the centre of stellar disk

$$I_j(x, s, \mu, t) = s_j \mu I_j(x) . \quad (1.66)$$

The total velocity of a projected surface element $\mu d^2s = r dr d\varphi$ is the velocity $v_j(t)$ of the star as before, plus projection μv_p of the pulsational motion into the line of sight. The broadening function given by (1.65) thus reads¹⁸

$$\Delta_j(x, t, p) = 2\pi s_j(t) \int \mu \delta(x - v_j(t) - \mu v_p(t)) r dr = \frac{2\pi R^2 s_j(t)}{v_p^3(t)} \left[(x - v_j(t))^2 \right]_{x \in (v_j, v_j + v_p)} . \quad (1.67)$$

Its Fourier transform reads

$$\tilde{\Delta}_j(x, t, p) = \frac{2\pi i R^2}{v_p^3(t)} s_j(t) \exp(iy v_j(t, p)) y^{-3} \left[\exp(iy v_p(t)) (2 - 2iy v_p - y^2 v_p^2) - 2 \right] , \quad (1.68)$$

it means, that in comparison with Eqs. (1.37) and (1.41) it contains now also additional broadening terms corresponding to the line-profile variations. A more detailed description of the disentangling with LPVs due to pulsations is given in recent publication (Hadrava, Šlechta & Škoda 2009).

Similar generalization can be done also for rotational broadening which causes LPVs in elliptic variables and can thus be found in the data. Non-zero limb-darkening leads in this case to asymmetry of lines and it complicates substantially the expression for Δ and its Fourier transform, equally as in the case of non-radial pulsations. However, Δ can be modelled and $\tilde{\Delta}$ calculated numerically in these cases.

¹⁸Here we use the relation $r dr = -R^2 \mu d\mu$. The bracket $[]$ in (1.67) means that the quadratic function inside is multiplied by the characteristic function of the interval in subscript (or interval $(v_j + v_p, v_j)$ if $v_p < 0$), i.e. by 1 inside and 0 outside the interval. Note that if the intensity in the lines is taken to be homogeneous instead of (1.61), the pulsational broadening is linear instead of quadratic and it thus leads to a smaller amplitude of observed pulsational Doppler shifts.

1.6.7 Rotational (Schlesinger – Rossiter – McLaughlin) effect

Another important case of line-profile (and consequent radial-velocity) variations is the rotational effect (Schlesinger 1909, Rossiter 1924, McLaughlin 1924) which may occur during eclipses.

Let us assume that the observed spectral flux is given by Eq. (1.64) with the broadening functions (1.65). Note, that it is customary (cf., e.g., Gray 2005, p. 436, 464 etc. as a classical reference) to simplify Eq. (1.64) to a single term ($k = 1$) for each component j , i.e. to assume the local intensity $I_j(x)$ to be the same function of x at each s and μ . This may be an acceptable approximation for some lines, however, it is incorrect to fix the limb darkening in lines to the values obtained for continua either from light-curve solution or from model atmospheres (cf. Hadrava 1997). Gray (2005, p. 436) argues that the limb-darkening coefficient “varies slowly with the wavelength and can be taken to be constant over the span of a spectral line”. However, this argument based on the behaviour of the limb darkening in continuum is incorrect, similarly as the slow (Planckian) variation of specific intensity in the continuum does not exclude its fast variation within the spectral line. It follows from calculations of μ -dependent synthetic spectra, that the limb-darkening varies across the line-profile and hence at least two terms (namely those proportional to μ^0 and μ^1) can fit strong lines like H α much better (cf. Hadrava and Kubát 2003).

On the other hand, we neglect here the coefficient $(1+v/c)^3$, which results from relation between the specific intensity and the Lorentz-invariant distribution function of photons (cf. Ohta et al. 2005), which, however is well negligible for non-relativistic velocities v .

We shall assume now, that the stars rotate with angular velocities ω_j as rigid bodies, their rotations do not oblate their spherical shapes and the gravity darkening is negligible, so that

$$I_j(x, s, \mu, t) = \sum_k \mu^k I_j^k(x) , \quad (1.69)$$

$$v_j(s, t) = \omega_j r_j v , \quad (1.70)$$

and

$$\mu = (1 - u^2 - v^2)^{1/2} , \quad (1.71)$$

where u and v are Cartesian coordinates on the projected visible stellar disc ($\mu d^2 s_j = r_j^2 du dv$). The coordinate u is chosen in the direction of projected rotational axis. If at time t the star j is partly eclipsed by star i with centre projected to coordinates $u_i(t), v_i(t)$, then the visible part of stellar disc s_j is given by conditions

$$u^2 + v^2 < 1 , \quad \text{and} \quad (u - u_i)^2 + (v - v_i)^2 < (r_i/r_j)^2 . \quad (1.72)$$

The broadening profile thus reads

$$\Delta_j^k(x, t, p) = \frac{r_j}{\omega_j} \int_{u \in s_j} (1 - v^2 - u^2)^{k/2} |_{v=x/r_j \omega_j} du . \quad (1.73)$$

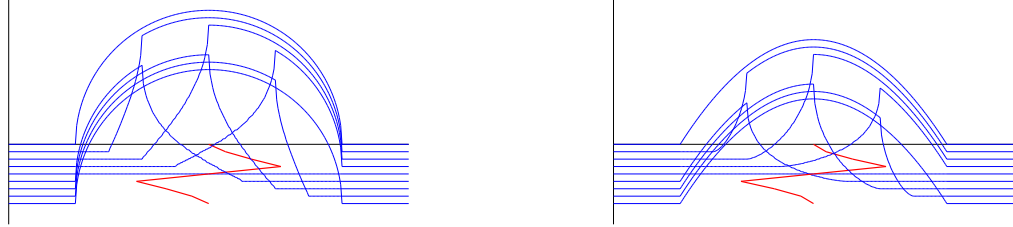


Figure 1.9: Broadening profiles Δ_j^0 (left) and Δ_j^1 (right) for a series of phases of total eclipse ($r_i = r_j$) with rotational axis perpendicular to the path of the eclipsing (i.e. the front) star. The broken line joining the profile centers indicates the observable RV-perturbation due to the rotational effect.

The first two of these broadenings have the form

$$\Delta_j^0(x, t, p) = \frac{r_j}{\omega_j} [u]_{v=x/r_j\omega_j, u \in s_j} \quad (1.74)$$

$$\Delta_j^1(x, t, p) = \frac{r_j}{2\omega_j} \left[u(a^2 - u^2)^{1/2} + a^2 \arcsin \frac{u}{a} \right]_{v=x/r_j\omega_j, u \in s_j} du, \quad (1.75)$$

where $a^2 = 1 - v^2$. Examples of these broadening profiles are shown in Fig. 1.9.

The standard treatment of the rotational effect does not deal with the shape of line-profile distortions during the eclipse, but with the resulting RV-shifts only. To assign an observed wavelength and hence also the RV to a spectral line with asymmetric profile is an ambiguous task. Different definitions are used, which imitate different methods of measurement – e.g. the wavelength of the extremal intensity (i.e. bottom of an absorption line) or centre of profile at half depth (or another fraction of the line depth) are taken. Here we use wavelength defined by Eq. (A.29) using the moments (calculated in the logarithmic scale) of line profile $\phi(x)$. An advantage of this definition is that the radial-velocity shift is additive with respect to subsequent broadenings of the profile. Let the broadened profile $\phi' = B * \phi$ arises from original profile ϕ by broadening B . Then according to Eq. (A.30) really the centre of the profile ϕ' is

$$x_{\phi'} = x_B + x_{\phi}, \quad (1.76)$$

where x_B is centre of the broadening profile B defined also by Eq. (A.29). It means that spectrographs with different instrumental profiles should give the same wavelengths (if their possible instrumental shifts x_B are subtracted), while the wavelengths given by alternative definitions depend on resolution. It is important to note, that centers of different broadening profiles Δ_j^k are generally different. Because different lines in spectrum of the same star are different superpositions of all of them, then the rotational effect may have different values for different lines.

1.6.8 Disentangling with constraints

It is obvious that from the view-point of generality of a model used for data interpretation as discussed in Section 1.2, the disentangling is less restrictive on the component spectra than the methods based on template spectra. On the contrary, in its standard form it is more restrictive regarding the broadening function compared to the Rucinski's method and, in some sense, even compared to any RV-measurement if the assumption of Keplerian motion is imposed on the disentangling (KOREL enables also arbitrary RVs for chosen components). Because each degree of freedom of the model can be useful or harmful for the solution depending on the particular case in question, it is desirable to have a tool for the data interpretation, in which the level of the model freedom could be tuned in details.

The above described generalization for line-profile variability enlarges the freedom of broadening function in the disentangling. It is thus needed to enable also some restrictions for component spectra. One straightforward possibility is to put a constraint on one or of the components in the form of template spectrum J_j (either from another star, from model atmospheres or even from other solutions of the same system) and to disentangle the observed spectra with respect to a subset of m component spectra only (and the parameters p of any broadening Δ_j) modifying Eq. (1.27) to the form

$$\sum_{j=1}^m I_j(x) * \Delta_j(x, t, p) = I(x, t) - \sum_{j=m+1}^n J_j(x) * \Delta_j(x, t, p) . \quad (1.77)$$

This may be useful e.g. for disentangling of telluric spectrum, which is basically known, but quite often its continuum is distorted due to an imperfect disentangling of lower Fourier modes of wide stellar lines.

Another type of constraints can be imposed on the orbital and other parameters of Δ -functions. Like in light- or RV-curve solution or any other data fitting, different parameters p can be either converged or fixed, if they are better determined by an independent way. However, a constraint on the parameters may also have a form of mutual dependence, which can be described by one or more conditions $F_k(p) = 0$ in the space of p . In such a case, the parameters can be substituted in a form $p = p(q)$ and the observations fitted with respect to the less dimensional space of q , or, invoking the method of Lagrange multipliers, the fit can be performed by numerical minimization of expression

$$0 = \delta \left\{ \sum_t \int |I - \sum_j I_j * \Delta_j|^2 dx + \sum_k \lambda_k F_k^2(p) \right\} , \quad (1.78)$$

where sufficiently high values of coefficients λ are chosen. The later approach is predominant, if the parameter constraints are also of an observational nature with some uncertainty. In such a case we can put $F^2 \equiv (O - C)^2$ and Eq. (1.78) is then an equation for simultaneous disentangling and solution of other type of data. A merging of disentangling (e.g. using KOREL) with solution of light- and RV- curves, astrometry etc. (e.g. using

FOTEL) is thus a direction to be followed in a near future (cf. Wilson 1979, Holmgren 2004, Hadrava 2004b, 2005).

1.6.9 Discretization of the input spectra

Both the contemporary observational technique of spectroscopy as well as the numerical data-processing on digital computers force us in practice to treat the stellar spectra not as smooth functions in the whole region of wavelengths but represented as a finite set of discrete numbers sampling the spectrum with limited spectral resolution within a limited spectral window. The detectors nowadays in use are mostly some CCD- or other electronic detectors, which integrate the light during the exposure in many pixels with individual characteristics of spectral sensitivity (hopefully linear in the intensity and very narrow-band, but never point-like in the wavelength). Depending on the spectrograph configuration, the individual pixels of detectors are usually arranged in the spectrograph focal plane both along the dispersion as well as in the transverse direction. The original data from the pixels are then (after a necessary flat-fielding etc.) interpolated to the desirable one-dimensional representation, usually calibrated in wavelength according to an exposure of properly chosen comparison spectrum. Similarly, the spectral resolution of previously used photographic spectrograms was limited by the finite size of emulsion grains in addition to the spectrograph limitations due to the slit-width or size and quality of the dispersion element, so that a scanning of the spectrogram yields again qualitatively comparable representation of the spectrum. Regarding the extension of the spectral window, it is usually limited by the spectrograph construction in combination with the size of detector (in addition to the limited spectral sensitivity of the detector and the transparency of the atmosphere and the instrument).

The discretized spectrum $D[I]$, which we use as an input for the disentangling method or for any other spectroscopic analysis is thus related to the original observed spectrum $I(x)$ by a relation, which can be expressed by means of a linear operator

$$D[I](x) = \sum_{k=1}^N \delta(x - x_k) D_k[I] \equiv \sum_{k=1}^N \delta(x - x_k) \int D_k(x') I(x') dx' , \quad (1.79)$$

where $\{x_k\}_{k=1}^N$ is the set of sampling frequencies (we assume $x_k < x_{k+1}$) and $D_k(x)$ is the overall spectral characteristic of sensitivity of the bin number k . For a simple approximation we can choose

$$D_k(x) \simeq \frac{x_{k+1} - x_{k-1}}{2} \delta(x - x_k) , \quad (1.80)$$

so that

$$D[I](x) = \sum_{k=1}^N \frac{x_{k+1} - x_{k-1}}{2} I(x_k) \delta(x - x_k) . \quad (1.81)$$

For an equidistant sampling ($x_{k+1} = x_k + \Delta_x$) we thus arrive at expression used for sampling e.g. by Gray (2005, p. 35), with the difference that the above expression includes also the limitation due to the finite spectral region (instead of $k \in (-\infty, \infty)$) and that it is multiplied by Δ_x to get $\int I(x)dx \simeq \int D[I](x)dx$ (and to preserve the same physical dimension of I and $D[I]$ also if x is not dimensionless). Another possible choice of the discretization, which better preserves the flux integrated over the frequencies is the box-function for D_k ,

$$D_k[I] = \int_{x_{k-1}/2+x_k/2}^{x_k/2+x_{k+1}/2} I(x)dx . \quad (1.82)$$

A more detailed model of discretization by a real exposure on a one-dimensional electronic detector (e.g. of the Reticon type) could be reproduced by a box-function narrowed for the width of gaps between the detector pixels. On the other hand, a misalignment of the detector with the dispersion or the instrumental profile of the spectrograph may cause a tail of D_k reaching even over several neighbouring pixels. These problems are particularly difficult in echelle spectrographs, where the tracks of individual orders are curved and thus necessarily also skewed with respect to the rows and lines of the matrix of detector pixels. When a one-dimensional representation of the echelle spectrum is obtained, value in each bin is a result of an interpolation between several detector pixels properly weighted to account for the blaze-function and the intensity profile in the direction of cross-dispersion of the orders (cf. e.g. Piskunov and Valenti 2002, Škoda et al. 2008 and references therein). Errors in this weighting, e.g. due to bad columns in the detector and a deformation between the exposure of the target star and the flat-field may induce a wavy patterns in the spectrum (cf. De Cuyper and Hensberge 2002, Hensberge 2004), which may then hamper the disentangling.

Despite the basic equations of the Fourier disentangling are valid for the spectra as functions of the logarithmic wavelength x regardless of their numerical representation, for practical reasons of computational performance the code KOREL uses the Fast Fourier Transform, which requires the data to be represented by values in equidistant spacing of x , the number of data points $N = 2^m$ (i.e. being given as an integer power of 2). Not to lose resolution by subsequent interpolations, it would thus be desirable to reduce the original read-out of the detector chip directly into the spacing required for the KOREL input. On the other hand, in view of all the above mentioned effects decreasing the spectral resolution, such an additional loss by interpolation is not substantial if the spacing of the KOREL input data is comparable or even better somewhat smaller than the resolution of the spectrograph. If we are forced to use a sparse data spacing significantly worse than that of the original data (e.g. in order to disentangle very wide spectral regions), the proper choice of the interpolation method may be important. The formula (1.82) preserving the integral flux is then advantageous, because the simple sampling (1.80) may skip narrow lines.

Hensberge et al. (2008) present the use of common sampling grid of all input data as a limitation of the Fourier method of decomposition “at the expense” of its efficiency.

This is misleading, because a rebinning is an inevitable feature of any method of the disentangling; once the input spectra are sampled in different grids and, moreover, for different components in the same exposure these grids are shifted for different radial velocities, resulting value in each bin of the disentangled spectrum must be a weighted mean of input values at wavelengths, which are generally interpolated between the grid points of input exposures. Fig. 1 by Hensberge et al. (2008) illustrates well that a common grid for all input exposures is taken in the standard wavelength-domain disentangling as well (cf. the original work by Simon and Sturm 1994). The numerical implementation of the method could be generalized in this respect, but, effectively, it would be equivalent to the resampling of the input. The problem is thus not which method to choose in order to minimize the loss by rebinning, but how to rebin the data optimally and the answer can be checked from the point of view of both these methods, which are equivalent in this respect. Regarding to the fact that the Fourier method solves the decomposition of spectra in terms of Fourier modes, just the Fourier modes of the input spectra are needed and these could be computed directly from the original sampling of the exposures. An interpolation scheme reproducing after FFT the same values of Fourier modes could thus be elaborated. A problem remains that the discretization decreases the amount of information in any case. It means, for instance, that some wavy patterns in the input spectra with frequencies in between the grid points could be filtered out, unless the representation will smear-out the input in terms of its power-spectrum.

A consequence of discretization of the spectra is the limitation of accuracy with which the radial velocities (and hence also the orbital elements) are determined. In the method by Simon and Sturm, the expected Doppler shift is rounded to an integer multiple of the radial-velocity step to determine the proper displacement of the unit off-diagonal. In the Fourier transform, the shift of the spectrum for value v is given by multiplication with function $\exp(iyv)$ (cf. Eq. (1.5)), which could be evaluated precisely at each frequency y , however, due to the limited number N of the modes taken into account, its inverse Fourier transform will generally produce a wider peak with some ghosts aside resembling interference fringes. Only in the special case of v being an integer multiple of the grid step, $\exp(iyv)$ is in resonance with the interval length in y -representation and a sharp shifted δ -function coinciding with a point of the x -representation can be reproduced. This is why the radial velocity is rounded to the nearest grid point in the Fourier disentangling also and why the radial velocities or their residuals calculated in the original KOREL-code are quantized depending on the radial-velocity step.

However, owing to the resolution in the digitalized values of intensity read from individual detector pixels, the position of spectral lines wider than the sampling step can be deduced with an accuracy exceeding the step width (cf. Fig 1.10). As described in the work Hadrava (2009), it is thus possible to reach a sub-pixel resolution in the disentangling. This method is implemented in the version KOREL08 of the KOREL code. Even higher precision could be reached in disentangling constrained by templates and the method could be applied in data-processing not only in spectroscopy.

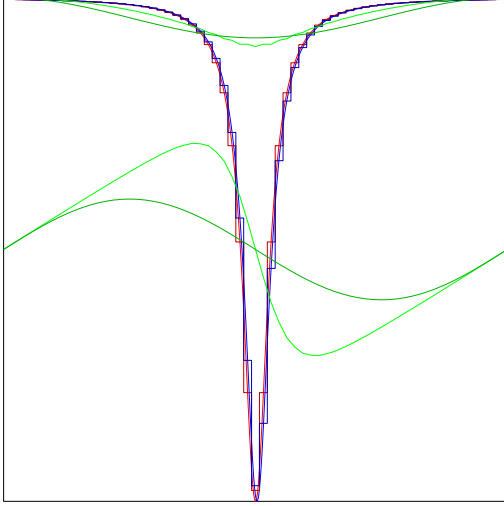


Figure 1.10: Discretization of a Lorentzian profile (the smooth thick line) centered with pixel position should yield a symmetric distribution of counts in neighbouring bins (the thick step function). A slightly shifted profile (for 0.2 pixel-width in this figure – see the thin lines) results in an asymmetry of the counts, which in turn enables to determine the position of the line with precision below the pixel width.

1.6.10 Normalization of disentangled spectra

Let us investigate now in detail the obstacle of the decomposition, which was already mentioned in Section 1.6.2 on page 28 and which is immediately obvious from Eq. (1.5). If we choose $y = 0$, the equation (1.5) received for the integral mean values $\int I_j dx$ reduces to a singular system of linear equations

$$\tilde{I}(0, t) = \sum_{j=1}^n \tilde{I}_j(0) . \quad (1.83)$$

According to the assumption of invariability of I_j in the simple disentangling, the mean intensity on the left-hand side of this equation should not depend on the time t . Assuming such a dependence to be caused only by a noise in individual exposures, the left-hand side can be replaced by its mean value, as it is done in Eq. (1.39). However, instead of a set of equations determining uniquely the other Fourier modes of component spectra, we have then this single condition restricting solutions for n values $\tilde{I}_j(0)|_{j=1}^n$ only to an infinite $(n - 1)$ -parametric set. In words it means that constant parts (continua) of the spectra cannot be decomposed, because they are invariant with respect to the Doppler shift. The continuum is never constant in the whole range of frequencies, so that in principle it should be possible to decompose the spectrum completely if it were to be available in the whole range of x with an unlimited precision. From the mathematical point of view it would require the use of additional conditions for limits, $\lim_{x \rightarrow \pm\infty} I(x, t) = 0$. In practice the whole spectrum is never available and its precision is insufficient to determine

the Doppler shifts of continua.¹⁹ Usually we decompose limited parts $x \in (x_1, x_2)$ of the whole spectrum which are rectified with respect to the local continuum. For these intervals the mean intensities

$$\tilde{I}_j(0) \equiv \langle I_j \rangle \equiv \int_{x_1}^{x_2} I_j(x) \frac{dx}{x_2 - x_1} \quad (1.84)$$

differ from the individual continua C_j . These differences can be found by a new rectification of the decomposed spectra, however the ratios of values C_j must be estimated from some additional information.²⁰ The uncertainty of C_j is also why KOREL gives the disentangled component spectra I_j on its output only relatively, i.e. in the same units used at input and with an unknown shift of the zero level (and of the continuum). Because the input spectra for disentangling are supposed to be rectified with respect to the total continuum (or a pseudocontinuum)

$$C \equiv \sum_{j=1}^n C_j = 1, \quad (1.85)$$

the output

$$I'_j(x) = I_j(x) - \langle I_j \rangle + 1 \quad (1.86)$$

is shifted for this value $C = 1$ to prevent negative values in absorption lines and to give an approximate information about the depths of the lines of individual components. However, to enable a comparison of the disentangled spectra with theoretical spectra from model atmospheres it would be desirable to calculate the component spectra rectified with respect to their (unknown) individual continua C_j , i.e. to find the functions $I_j(x)/C_j$.

The only value we can calculate from the input spectra is the total mean intensity

$$\langle I \rangle = \sum_{j=1}^n \langle I_j \rangle. \quad (1.87)$$

This value (which is decreased below the level of total continuum for the ratio of sum of equivalent widths of lines in the spectral region and the length of the region) is given at the output of KOREL for each spectral region. Even if we know, e.g. from a broad-band photometry, the ratio of colour luminosities

$$L_j = \int I_j(x) \phi(x) dx \quad (1.88)$$

¹⁹In fact just such an overestimation of the effect was a shortcoming of the historical paper by Christian Doppler (1842).

²⁰As it has been mentioned already in Section 1.6.2, the sets of linear equations (1.5) may be nearly singular also for some other low harmonics and due to the limited precision of the source data their solution may be unstable, especially if the radial velocities are not yet well converged. This results in some long-period waves on the decomposed spectra, which are frequently met during the procedure of convergence of the disentangling. Usually these waves disappear when a better solution is reached, however, a better rectification of the input spectra can also help.

of the components, it does not tell us directly the ratio of $\langle I_j \rangle$, because L_j are integrated over a broader region with wavelength-dependent sensitivity ϕ of the photometric channels (given by filters/detectors). Both integrals (1.84) and (1.88) are decreased with respect to the levels of continua C_j by the sum of equivalent widths of absorption spectral lines contained in the corresponding region. However, for disentangling we usually choose narrow neighborhoods of strong (mostly absorption) lines, so that the values of $\langle I_j \rangle$ can be expected to be sensibly smaller in comparison with levels of continua C_j , while the photometric luminosities can nearly reach the values of integrals of the continua²¹

$$\langle I_j \rangle < C_j, \quad L_j \leq C_j. \quad (1.89)$$

Fortunately, the shifts of components' mean intensities with respect to their continua can be determined from the output disentangled spectra

$$\Delta_j \equiv C_j - \langle I_j \rangle = [I'_j(x) - 1]_{x \in \text{cont.}} \quad (1.90)$$

(cf. Eq. (1.86)) simply by fitting the level of continuum in I'_j . These n values should satisfy the bounding condition which follows from Eqs. (1.85) and (1.87),

$$Q \equiv 1 - \langle I \rangle - \sum_{j=1}^n \Delta_j = 0, \quad (1.91)$$

the right-hand side of which is given at the output of KOREL as the integral of the input spectra. Neglecting this condition, the continuum shift of each disentangled component spectrum could be calculated independently by a new rectification of the output as its mean value in the continuum. Such a result could be then substituted into Eq. (1.91) to check it precision. An alternative approach is to solve for all Δ_j simultaneously by minimizing the sum

$$S \equiv \sum_j w_j \int [I'_j(x) - 1 - \Delta_j]^2 \quad (1.92)$$

with the condition (1.91). Here the weight w_j of each component spectrum can be chosen inversely proportionally to the square of its noise. The minimization can be done using the standard Lagrange multipliers method, i.e. solving the set of linear equations

$$0 = \frac{\partial}{\partial \Delta_j} [S - \lambda Q] = 2w_j \int [\Delta_j + 1 - I'_j(x)] - \lambda. \quad (1.93)$$

The solution reads

$$\Delta_j = \left(\int [I'_j(x) - 1] + \frac{\lambda}{2w_j} \right) / \int 1, \quad (1.94)$$

²¹The correction could be obtained from model atmospheres. In the next we will thus suppose that we know the ratio of the continua C_j from the photometry.

where

$$\lambda \sum_j \frac{1}{2w_j} = [1 - \langle I \rangle] \int 1 - \sum_j \int [I'_j(x) - 1] . \quad (1.95)$$

Once the shifts Δ_j are determined (and continua C_j chosen), the rectified component spectra can be calculated according to

$$I_j(x)/C_j = 1 + (I'_j(x) - 1 - \Delta_j)/C_j . \quad (1.96)$$

Note, that a telluric component contributes also by its Δ_j , despite it has $C_j \equiv 0$ (but its $\langle I_j \rangle < 0$). It is natural to let the telluric lines be normalized with respect to the total continuum C .

1.6.11 Numerical method

The Fourier transform is calculated in KOREL using the procedure Fast Fourier Transform (FFT). Consequently, the input spectra must be discretized into 2^n points equidistant in logarithmic wavelength.²² The shift ($v_j(t)$) of δ -function in Eq. (1.4) or its generalizations must be discretized with the sampling frequency (to give the function $\exp(iyv_j(t))$ in Eq. (1.5) periodic with the period of the data interval). Consequently, both $v_j(t)$ as well as the minimized sum S given by Eq. (1.32) are step functions (in t and p , resp.) in the numerical representation. To achieve a good resolution in velocity, it can thus be advantageous to interpolate the input spectra into higher sampling density than the original one read from the detector. The Fourier transforms of these spectra must be stored in the computer memory in the course of the solution. To enable the use of large number of spectra with high resolution, the spectra can be represented by several spectral regions only (containing spectral lines chosen for the solution), each one characterized by the initial wavelength and step in radial velocity per one bin. For each spectral region the functions S are calculated according to Eq. (1.32) and the corresponding sets of Eqs. (1.42) are independent. The total S summed over spectral regions is calculated only for the purpose of convergence of parameters p .

The spectra are supposed to originate from a multiple stellar system with a hierarchical structure shown in Fig. 1.11, where the numbers in circles are indexes of the star position, numbers in parenthesis give indexes of the corresponding orbit. The occupation of each position by a visible component is to be given by special key on input. The orbits Nos. 1, 2 and 3 can be suppressed by the choice of the corresponding period equal to 0.

The radial velocity of a component is thus given by

$$v_j(t; p) = \sum_o K(\cos(\omega + v) + e \cos \omega) , \quad (1.97)$$

²²The number of data points in each spectral region is 256 in the PC-version or its multiple by a power of 2 in the workstation version of the code KOREL.

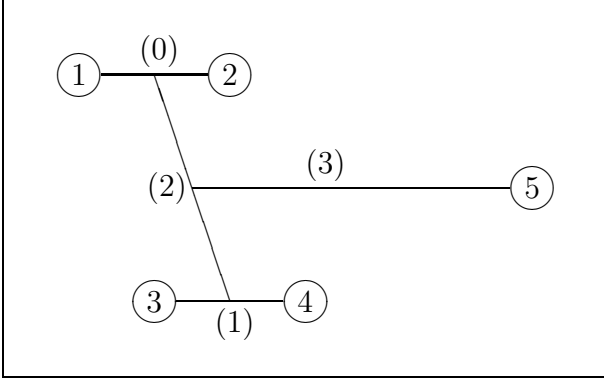


Figure 1.11: The hierarchical structure of the stellar system. The numbering of component stars (in circles) and their orbits (in parenthesis) as used in KOREL is shown.

where the summation is performed over the orbits influencing the motion of the star (e.g. orbits Nos. 0, 2 and 3 for the star No. 1; note that the γ -velocity of the system does not appear in this formula – it can be specified only after the identification of lines in the component spectra). The true anomaly v is calculated according to

$$v = 2 \arctg \left(\sqrt{\frac{1+e}{1-e}} \operatorname{tg} \frac{E}{2} \right) \quad (1.98)$$

from the solution of Kepler's equation

$$2\pi \frac{t - t_0 - \Delta t}{P} \left(1 - \frac{\dot{P}}{2} \frac{t - t_0 - \Delta t}{P} \right) = M = E - e \sin E \quad (1.99)$$

for the time t corrected by

$$\Delta t = \sum_o \frac{PK}{2\pi c} (1 - e^2)^{3/2} \frac{\sin(\omega + v)}{1 + e \cos(v)}, \quad (1.100)$$

for the light-time effect due to the higher orbits in the hierarchical system (e.g. orbits Nos. 2 and 3 for stars Nos. 1 and 2). The pericenter longitude is given by

$$\omega = \omega_0 + \dot{\omega}(t - t_0 - \Delta t), \quad (1.101)$$

i.e., the secular periastron advance (linear in time) can be taken into account. Similarly

$$e = e_0 + \dot{e}(t - t_0 - \Delta t), \quad (1.102)$$

$$K = K_0 + \dot{K}(t - t_0 - \Delta t), \quad (1.103)$$

$$q = q_0 + \dot{q}(t - t_0 - \Delta t), \quad (1.104)$$

The spectra and times of exposures are usually transformed into the heliocentric system. If not, the higher orbit can be used to make the corresponding correction. The

secondary component of this ‘solar’ orbit can be used to remove the telluric lines (in an approximation) from the stellar spectra.

The minimization of S with respect to p is performed by the simplex method adapted from Kallrath and Linnell (1987).²³ Several orbital elements (cf. Table A.1), line strengths²⁴ or radial velocities²⁵ can be chosen from all of them for convergence in one step, the others being fixed. In each of these ‘large’ steps, there are performed many simplex transformations. The number of these ‘small steps’ is $10\times$ the number of the iterated parameters (at maximum 10 parameters can be converged in one large step). The actual status of the iteration is displayed on the screen (in order: No., code of simplex transformation, No. of the worst simplex point, value of S in this point and its values of parameters, i.e. in the same way as in FOTEL). At each simplex step the spectral decomposition is performed first, and then the line-strengths are calculated (if it is required by the corresponding key of the star). The self-consistent solution requires either to repeat these steps, or to store the values of line-strengths appropriate to the set of orbital parameters at a particular simplex point. The former approach is used in the present version of KOREL because the later would be memory exhausting. To find an exact self-consistent solution in each step would be very time consuming, hence only up to 5 iterations of successive spectra decomposition and line-strengths calculations are performed. The solution with free line-strengths is usually more sensitive to local minima in the basic parameters. To prevent this disadvantage it is recommended to hold the line-strengths fixed during the simplex solution (unless it is only tiny tuning of an already found solution) and to improve them in a subsequent step. Another possibility is to include some line-strengths (of chosen components in chosen exposure – e.g. very strong telluric lines or components participating in an eclipse) between the parameters converged by simplex with other line-strengths held fixed.

For the purpose of different numerical tests, there is built-in into KOREL a possibility to produce synthesized data with chosen orbital parameters. The profiles of each component can be then chosen in one of two types, either with broad wings (type 1)

$$I_j = -c \frac{\Delta^2}{(x - x_0)^2 + \Delta^2}, \quad (1.105)$$

or with continuum (type 2)

$$I_j = c \min \left[0, \left(\frac{(x - x_0)^2}{\Delta^2} - 1 \right) \right]. \quad (1.106)$$

Random noise of a chosen amplitude can be added into each bin.

²³For details see description of the code FOTEL (Hadrava 2004b in this volume), where the same procedure is used.

²⁴Note that either all line strengths for a chosen component can be calculated using the method described in Section 1.6.3, or only several of them (e.g. in exposures suspicious to be taken during an eclipse) using the simplex method.

²⁵For a component which is not tied to an orbital motion – cf. *KEY* explained in Section A.3.2.

Chapter 2

Practice of spectra disentangling

2.1 Practical conditions for the use of KOREL

In this part of the text, a guide to practical exercises prepared for afternoon sessions of the Summer school is provided. These exercises simulate the future practical use of the code KOREL.

Each group is provided with an account and a terminal, i.e. a workstation with Linux Debian and GNOME environment (KDE and XFCE4 are also installed) in a local net with a central disc-field. (It means that the users may log in at any terminal.) The usernames are `korel01`, `korel02`... `korel12` and the corresponding passwords `01noh`... `12noh`. (The passwords should not be changed and everybody should use his own account only.) The terminal windows can be opened e.g. in menu **Application** → **Accessories** → **Terminal** or by an icon on the top bar (FIREFOX, GEDIT, DOSEMU and GEDIT are also on the bar). The standard applications like SSH, SCP may be used from there to reach remote computers, editors VIM, GVIM, GEDIT or KEDIT (also available at **Application** → **Other** → **KEdit**), or PostScript viewers EVINCE or GV. A nonstandard but needed is DOS-emulator (available in **Application** → **System tools** → **DOS emulator** or by the icon on the bar), which works at the C: directory available in LINUX at directory `./dosemu/drive_c`.

Another account with the same user-name is provided at the Ondřejov cluster of computers

`***.cz`, IP address `147.***`.

The password `***01` corresponds to username `korel01` and the last two digits are to be replaced correspondingly for other users. In the home directories of the users are prepared executable codes of KOREL and other LINUX-codes. There are also exe-versions of codes running in DOS only, which we shall download via SCP to the local C: directory.

At the cluster the subdirectories `/exe1`... with data for the exercises are also prepared. These will be used either directly at the cluster, or they will be downloaded to the local terminal first and results from the work with them will be sent back, like in future data

prepared from the users own observations.

The data on real stars which are prepared for the exercises originate mostly from the Ondřejov 2m- telescope and they were observed for studies either already published in the past or intended in future. It means that the data should not be used for other purposes than the training without a special agreement with their authors. The data are not provided as complete sets and their reduction is not always the best as required for real scientific use. On the other hand, some of them were chosen with regards to personal interests of the participants, so that it is possible that a future cooperation combining Ondřejov and other data could be welcome.

2.2 An easy start with KOREL

To perform the disentangling in its simplest form, we have to provide the KOREL-code with:

- (1) the spectra to be disentangled,
- (2) with initial estimates of the parameters of the system and
- (3) with codes controlling the run of the code.

(Other possibilities will be shown later.) The spectra are to be given in the input file `korel.dat`, the parameters and codes in `korel.par`, both in the format described in the Manual in Sections A.3.3 and A.3.2, resp.

The choice and preparation of the spectra may be a laborious task for which an auxiliary code PREKOR is written and its use will be explained later. The main demands are that the input spectra should be sampled in the same equidistant grid of logarithmic wavelength-scale (with 2^n grid points, n being integer; a reasonable minimum is 256) and they should be rectified to the continuum. In the chosen spectral region it is desirable to comprise the same lines in all exposures and to have a continuum at the edges of the region. To solve for orbital parameters, a maximal resolution around well visible lines is preferred (e.g. one line only), while for the purposes of analysis of the disentangled spectra we can choose longer regions with a smaller resolution (and to keep the orbital parameters fixed from a previous solution of high-resolution regions of spectra).

A proper formulation of the questions given to KOREL in the file `korel.par` is the core of the art of disentangling. KOREL is not an expert system analyzing the input in an automated way and the user has to involve his own intuition to estimate which questions could be answered from which data in which order and to judge if the results are reasonable and enable one to ask more. Usually we know or at least we suspect what the orbital parameters of the studied object may be (e.g. the period may be known from a photometry) and their uncertainties. We have to include these values on input and to decide which of them may be improved using our data. We have also to decide from both the output values of parameters and the disentangled spectra if the result may be correct and if it hit an acceptable solution.

2.2.1 Example 1 – simulated data

Here, we shall start first with disentangling of simulated spectra, which have the advantage that we know what their chosen properties are and we may check how well they are restored by the disentangling. KOREL includes an option to create simulated data, however, they cannot be saved. In the directory `EX1` we have data (in the file `kor0801a.dat`) created by an independent code. They approximately repeat those on which the function of KOREL was demonstrated in the first publication (Hadrava 1995). There are simulated 7 exposures covering uniformly one period of a double-lined binary on a circular orbit with semiamplitudes of radial velocities $K_1 = 22$ and $K_2 = 44$ km/s. The calculated

spectral region is sampled in 256 bins with a step of 2 km/s, contains one line composed of Lorentzian profiles with central intensities in ratio 4:1 and semi-widths corresponding to radial velocities 40 and 70 km/s for the primary and secondary, respectively. An artificial noise is added to the signal with an amplitude up to $\pm 2\%$ of the continuum. The data-file begins with a line giving the time of the exposure (here it runs from .0000 to 1.0000; we chose the period to be 1.), initial wavelength (in Å, here chosen arbitrarily) and step of the sampling in km/s of the spectral region, weight of the exposure (chosen here 1.000 for all exposures) and the number of bins (here 256) in one exposure. Then follow the values of the intensity in these bins – cf. the file `kor0801a.dat`, which we shall copy now to the file `korel.dat`:

```
.0000 4500.0000 2.000 1.000 256
.99143 .97534 .98784 .98352 .97205 .98681 .98670 .99434 .98397 .98431
.96184 .97731 .98497 .99025 .97306 .97125 ...
```

The file with corresponding parameters and controlling codes for decomposition of these profiles is prepared as `kor0801a.par`, from where we shall copy it to `korel.par`. Its complete form reads:

```
1 1 0 0 0 1 0 2 2      |key(5), k= Nr. of spectra, filter, plot, print
o 0 1 0 1 1 1. 0.001   = PERIOD(0)
o 0 2 0 1 1 0. 0.1     = PERIASTRON EPOCH
o 0 3 0 1 1 0. 0.1     = ECCENTRICITY
o 0 4 0 1 1 0. 10.     = PERIASTRON LONG.
o 0 5 0 1 1 22. 5.     = K1
o 0 6 0 1 1 .5 0.1     = q = M2/M1, K2 = 44.
x 0 0 0 0 0 0 0        | end of elements
```

Here the digits 1 between the first five numbers specify that the spectra of components 1 and 2 from the hierarchical structure shown in Fig. 1.11 are present, while the other three are not. Subsequent 6 lines give the values of orbital parameters of this pair (in the seventh column). We do not request their convergence (as given by zero in the fourth column). The last line denotes end of the input of parameters. (See Section A.3.2 for a complete explanation of the file `korel.par`.)

Having prepared both files `korel.dat` and `korel.par`, we can run now the code `korel08`. It produces numerical results in the file `korel.res` and a graphic output in the file `phg.ps`, which we can see in Fig. 2.1. We can see here that the disentangling is able to separate the profile of the secondary component from the phase-locked variations of asymmetry of the apparent single peak seen as a result of the blending in the input spectra and to restore also the symmetric profile of the primary.

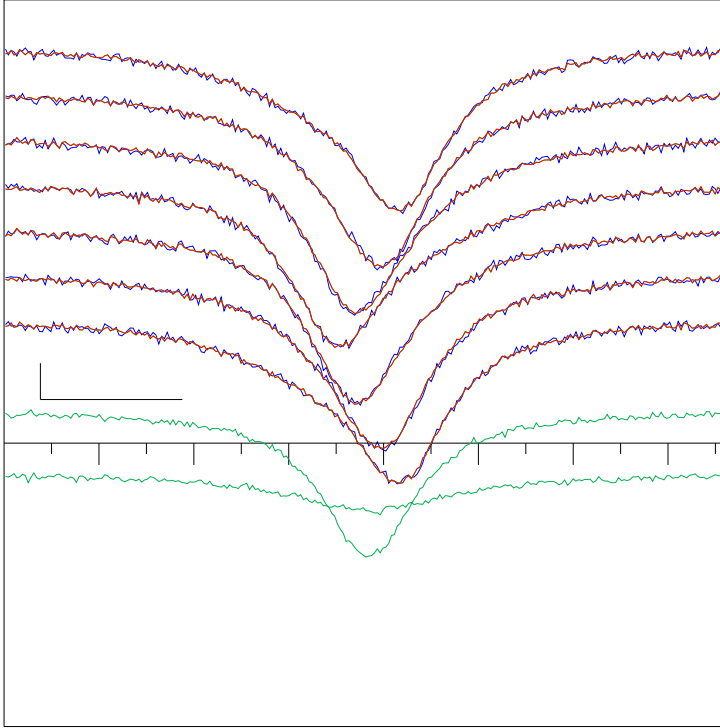


Figure 2.1: Simulated composite line profiles (7 blue upper curves) of a binary from the file `kor0801a.dat`, the disentangled component spectra (2 bottom green curves) and their superposition on the input profiles (red lines).

However, this run of KOREL was a simple decomposition and not a full disentangling, because the orbital parameters were fixed to their exact values, which we know from the simulation of the data. It can be seen in Fig. 2.2 how the χ^2 of the residual noise depends on the amplitudes of radial velocities if we fix them for the component stars to different values for the file `kor0801a.dat` and also for `kor0801b.dat`, which is simulated with the same parameters of the orbit and line profiles, but the random noise is 10-times smaller. It is obvious that the minimum is much deeper and its position more precisely defined for the data with smaller noise.

To simulate a real case of disentangling of spectra for systems for which the orbital parameters are not well known, we shall change the initial values of some parameters and then we shall let them converge. For instance, let us change three lines in the file `korel.par` as follows:

```
o 0 2 02 1 1 0.1 0.1    = PERIASTRON EPOCH
...
o 0 5 01 1 1 12. 5.     = K1
o 0 6 01 1 1 .3 0.1     = q = M2/M1,  K2 = 44.
```

If we shall run now FOTEL again, it will show on the screen and also in the output-file `korel.res` a protocol about simplex convergence of the parameters in the form:

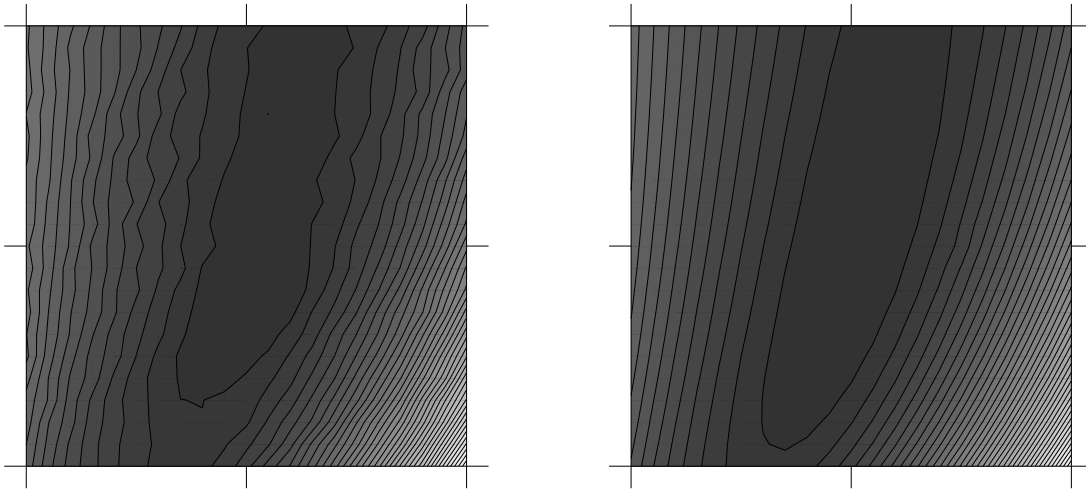


Figure 2.2: Residual noise as a function of K_1 and q for data from the file `kor0801a.dat` (left) and `kor0801b.dat` (right).

```

1 C 2 0.36407E+03 0.19428E+00 0.13179E+02 0.32357E+00
2 A 4 0.21356E+03 0.12357E+00 0.13179E+02 0.39428E+00
3 A 3 0.21257E+03 0.12357E+00 0.16714E+02 0.32357E+00
4 B 1 0.17167E+03 0.10000E+00 0.12000E+02 0.30000E+00
5 B 3 0.10573E+03-0.55232E-01 0.12471E+02 0.30440E+00
6 A 1 0.72220E+02 0.20518E-01 0.13715E+02 0.30971E+00
7 B 2 0.59546E+02-0.25708E-01 0.15378E+02 0.36757E+00
...
30 A 2 0.20125E+02 0.94115E-04 0.21837E+02 0.43925E+00
31 3 0.20125E+02 0.77977E-05 0.20220E+02 0.52600E-04
31 4 0.20125E+02 0.98819E-04 0.21835E+02 0.43926E+00

```

It is natural that the wrong starting values of parameters resulted in a much higher residual sum – instead of about 20.76 in the correct solution to 171.67 in the starting point (see the fourth line) or even to 364.07 in the first line which has the largest deviation in the time of periastron. However, the simplex converges finally to values, which by chance fit the spectra with their noise even better (20.125) than the true values. The time of periastron is restored with an error about 10^{-4} of the orbital period, K_1 with error about 1%, but the

mass ratio (and hence also K_2) about 10%. This is obviously due to the fact, that the the line of the secondary is wide and shallow and hence the minimum of O–C in Fig. 2.2 has a shape of a valley elongated in the q -direction with poorly distinguished deepest point. The same calculation with the less noisy data from `kor0801b.dat` restore the true values of parameters much better. If we fit q to some wrong value (e.g. 0.3), we get still quite satisfactory solution. Another interesting experiment is to disentangle the data a single-line binary, i.e. to change the first line of `kore1.par` to: `1 0 0 0 0...` and naturally to skip a convergence of q . The K_1 velocity then converges to the value about 14.54 km/s. It shows that the disentangling is sensitive more to the bottom of line-profile, because the radial velocity defined by moments has amplitude $(22*4*40-44*1*70)/(4*40+1*70) \simeq 1.91$ km/s only. Nevertheless, the unresolved secondary apparently decreases the amplitude (22 km/s) of the primary line.

2.2.2 Example 2 – 96 Her

In files `kor0802a.dat`, `kor0802b.dat` and `kor0802c.dat` in the directory `EX2` we have prepared three regions of the star 96 Her. Corresponding values of parameters with well progressed solutions are in files `kor0802a.par`, `kor0802b.par` and `kor0802c.par`.

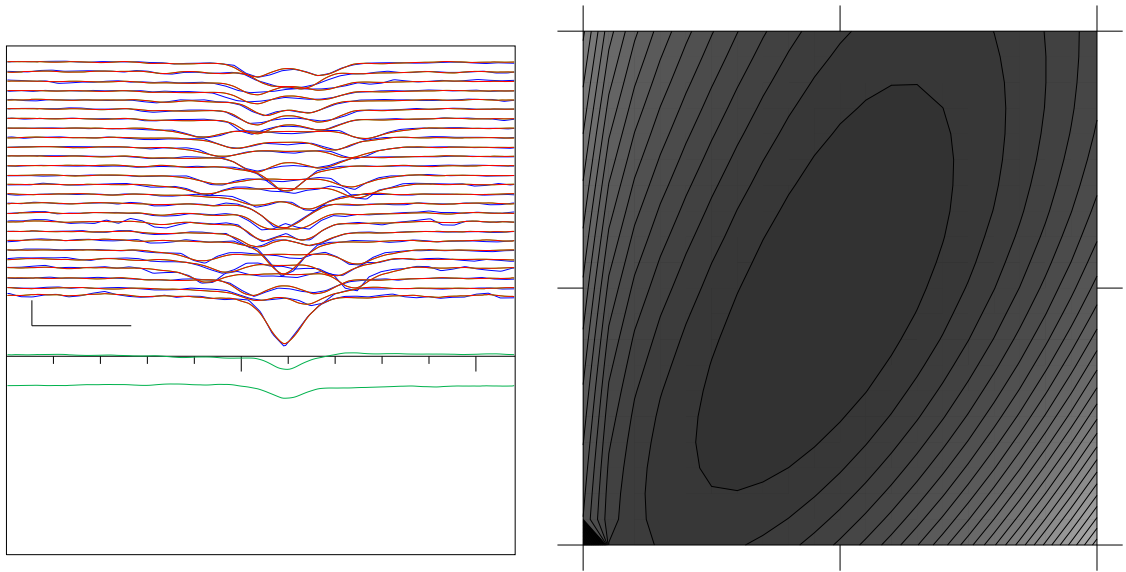
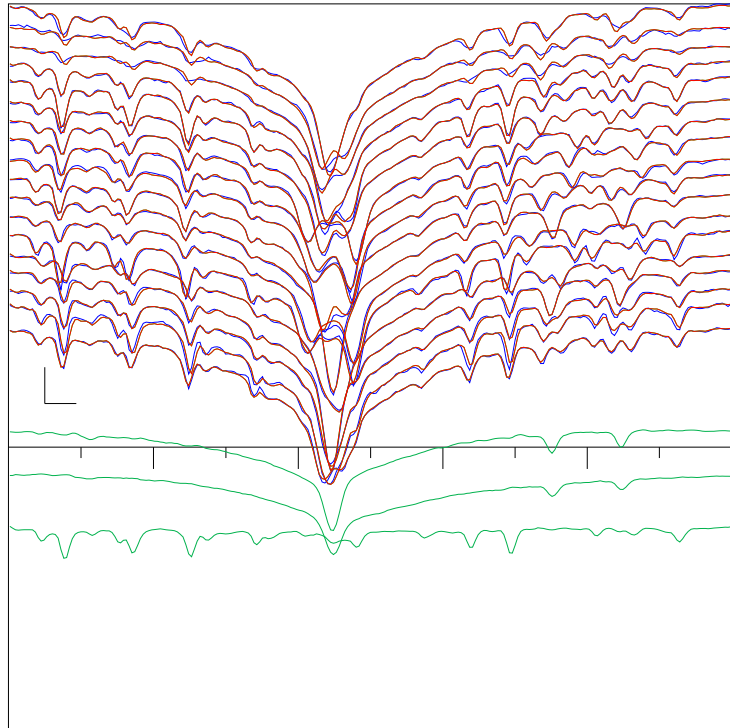


Figure 2.3: Disentangling of 96 Her from the file `kor0802b.dat` (left) and residuals from `kor0802a.dat` as a function of K_1 and q (right).

Figure 2.4: Disentangled H_α from the file `kor0802c.dat` (the primary, secondary and the telluric component).



2.2.3 Example 3 – 55 UMa

In the directory `EX3` we have prepared several spectra of the triple star 55 UMa in the form of ASCII table. We have to prepare the input `kore1.dat` and `kore1.par` using the code PREKOR. PREKOR runs under the DOS and its executable version `prekor14.exe` can be downloaded from the main directory. We shall download it into the C: directory of the DOS-emulator, equally as the spectra (`55u0*.asc`), their list `prekor.lst`, which also provides the Julian dates of these exposures, and the file `prekor.par`. In the C: directory we can run PREKOR, either in the option “0” to calculate the orbital parameters for disentangling the telluric lines (they are contained in the output file `prekor.res`), or with some higher number, to produce the data `kore1.dat` (in the output `prekor.out`). This output will be sent back to the cluster. Before it can be run by KOREL, it must be converted from the DOS-format into the UNIX format. This can be done, in principle using the utility `dos2unix` (not available here), or using the trick recommended by Bajur Indradjaja, i.e. by the command `tr -d "\r" < input > output`, or using the code KORTANS (cf. Section A.3.6).

2.3 Rectification of the input spectra

2.3.1 Example 4 – α CrB

The FITS-files of unrectified spectra of the binary α CrB (Gemma) are given in the directory **EX4**. The rectification may be performed using my code **REKTIF** (cf. A.3.5 on p. 214), the DOS exe-version of which can be downloaded from the main directory. The input spectrum is supposed in the form of ASCII-table, so we need also to convert it at first. This is possible using the code **FIT2ASC.exe**, which can also be downloaded from the main directory. Each spectrum is to be copied to the file **fit2asc.in**, then a run of the **FIT2ASC**-code creates the output table in the file **fit2asc.out**. The first lines may contain JD if it is given in the header of the FITS-file (it is to keep some identification of the exposure. This output should be copied (or renamed) to the file **rektif.dat**. We also need to prepare the file **rektif.par** defining the procedure of the rectification. To specify the window in wavelength and values of signal, we may either check these quantities from the input-file **rektif.dat**, or we can run the code with any values and read them from the output **rektif.res**. In the file **rektif.par** we also have to specify initial values of the continuum-marks. Provided we do not have any better estimate, we can chose the signal level at the maximum and set the acceptable error close to 100% (1.0).

2.3.2 Example 5 – 68 u Her

In the directory **EX5** data and example of solution are presented for another system to which I applied **KOREL** already in its beginning. Participants of the School may try their own creativity how to treat these data.

Appendix A

Appendices

A.1 Historical background

The method of disentangling, equally as other methods dealing with observations of spectroscopic binaries, is based on Doppler principle. Application of this principle is nowadays so widely spread in different fields not only of science but also of technical or medicine practice, that it is little known that the original idea which motivated the Austrian physicist Christian Doppler (1803-1853) to suggest his principle was just an attempt to explain observations of binary stars. In his seminal work “Über farbige Licht der Doppelsterne und einiger anderer Gestirne des Himmels” (“On the coloured light of the double stars and certain other stars of heavens”, cf. Doppler 1842) presented on 25th of May 1842 to six listeners only at a session of the Royal Bohemian Society of Sciences in the Patriotic Hall of Prague Karolinum, he tried to explain differences between colours of components in some visual binaries by shifts of frequencies of light due to the different radial velocities of the stars.



Christian Doppler



W. H. Wollaston

Doppler’s ingenious (but quantitatively exaggerated) idea was modified in 1848 by French physicist Armand-Hippolyte-Louis Fizeau (1819-1896), who showed the frequency shift in acoustics. Being unaware of Doppler’s work, Fizeau predicted that the same effect should be observable for light and that a tiny shifts of absorption lines in stellar spectra could reveal the velocities of stars. Such absorption lines were observed first in the solar spectrum by English versatile scientist William Hyde Wollaston (1766-1828) in 1802 and then by the German optician Joseph von Fraunhofer (1787-1826) in 1814, but they were explained by German physicists Robert Wilhelm Eberhard Bunsen (1811-1899) and Gustav

Robert Kirchhoff (1824-1887) in 1859 only.

In 1863, Italian Jesuit astronomer Pietro Angelo Secchi (1818-1878) started to investigate systematically the spectra of stars for the purpose of their spectral classification (introduced by him) with an intention to measure also their motion, which, however, was beyond the capability of his spectrograph. The first measurement of radial velocity was performed in 1868 for α CMa by English spectroscopist Sir William Huggins (1824-1910), who investigated (from 1864) spectra of star and nebulae also in order to determine their chemical composition by identification of their spectral lines.

The German astronomer Hermann Carl Vogel (1841-1907) used the Doppler principle to measure spectroscopically the rotation of the Sun in 1871, to compile a catalog of radial velocities of 51 stars between 1871 and 1892 and to identify as spectroscopic binaries the stars β Per (explained already in 1783 as an eclipsing binary by John Goodrick, 1764-1786) and α Vir in 1889.

In the same year 1889, another spectroscopic binaries, ζ UMa and β Aur were discovered also by American astronomers Edward Charles Pickering (1846-1919) and Antonia Caetana Maury (1866-1952).



H. C. Vogel

No matter how remarkable is the history of the observational astrophysics, for a true progress in understanding of Nature are essential the theoretical conceptions, which enable to rise appropriate question, to find an efficient way to answers and to make reasonable conclusions. A backbone of exact sciences is the mathematics, which is able to yield answers even long time before the questions arise.



J. B. J. Fourier

This is also the case of the Fourier disentangling of spectra, which is based on the transform introduced by the French mathematician Jean Baptiste Joseph Fourier (1768-1830) well before the problem of the Doppler shift could be settled. Fourier transform has many applications not only in solving the differential equations (Fourier introduced it to solve equation of heat conduction) by the so called spectral methods (or harmonic analysis) but also for computing and processing of signal in different technical applications.

One of these applications is also the computer tomography, which enables to reconstruct spatial distribution of sources from different projections of their emission. This technique is based on the Radon transform and its inverse, which was introduced by the Austrian mathematician Johann Radon (1887-1956). In the form of the so called Doppler tomography, it is also applied in stellar spectroscopy and it is related to the disentangling of spectra as well.

Some basic conceptions of this mathematics necessary for understanding of the spectra disentangling will be reminded in the next Section.

A.2 Mathematical background

A.2.1 Fourier transform

Fourier transform of a complex function $f(x)$ of real variable x (to the complex function $\tilde{f}(y)$ of real variable y) is given by

$$\tilde{f}(y) = \int_{-\infty}^{\infty} f(x) \exp(ixy) dx , \quad (\text{A.1})$$

and its inverse transform

$$f(x) = \frac{1}{2\pi} \int_{-\infty}^{\infty} \tilde{f}(y) \exp(-ixy) dy . \quad (\text{A.2})$$

It should be hold in mind that different normalizations are used in the literature – e.g. $\mathcal{F}[f](\sigma) = \int f(x) \exp(2\pi i x \sigma) dx$ (Gray 2005, p. 26), for which the inverse transform is $f(x) = \int \mathcal{F}[f](\sigma) \exp(-2\pi i x \sigma) d\sigma$, or $\mathcal{F}[f](y) = \tilde{f}(y)/\sqrt{2\pi}$, which has the same normalization factor at its inverse. Our asymmetric choice corresponds to the practice in use of the numerically effective algorithm of Fast Fourier Transform (FFT).

Obviously, Fourier transform of a real function has an even (symmetric) real part and odd (antisymmetric) imaginary part

$$\tilde{f}(-y) = \tilde{f}^*(y) , \quad (\text{A.3})$$

where the asterisk $*$ denotes the complex conjugate ($(a+ib)^* \equiv a-ib$, for a, b real). Fourier transform is linear (with respect to the addition of functions and their multiplication by a complex constant). Rescaling of a function in the x space corresponds to the inverse rescaling in the y space

$$\tilde{f}\left(\frac{y}{a}\right) = a \int_{-\infty}^{\infty} f(ax) \exp(ixy) dx . \quad (\text{A.4})$$

According to the Parseval theorem, the norm of a function (defined by $\|f\|^2 \equiv \int f^*(x)f(x)dx$) is proportional to the norm of its Fourier transform

$$\begin{aligned} \int |\tilde{f}(y)|^2 dy &= \int \tilde{f}^*(y) \int \exp(ixy) f(x) dx dy = \int f(x) \left[\int \tilde{f}(y) \exp(-ixy) dy \right]^* dx = \\ &= 2\pi \int |f(x)|^2 dx \end{aligned} \quad (\text{A.5})$$

(i.e. the norm $\|f\|$ is preserved up to the multiplicative constant $\sqrt{2\pi}$ in our normalization). Consequently, the Fourier transform also preserves (up to the same constant) the scalar product of functions defined by $(f, g) = (\|f + g\|^2 - \|f\|^2 - \|g\|^2)/2 = \int (g^* f + f^* g)/2 dx$.

It is crucial for the application on the disentangling of spectra that for a convolution of two functions defined by

$$h(x) \equiv [f * g](x) \equiv \int_{-\infty}^{\infty} f(x-v)g(v)dv , \quad (\text{A.6})$$

the Fourier transform is a simple product of the transforms

$$\begin{aligned} \tilde{h}(y) &= \int \int f(x-v)g(v)dv \exp(ixy)dx = \\ &= \int f(x-v) \exp(i(x-v)y) d(x-v) \int g(v) \exp(ivy)dv = \tilde{f}(y) \cdot \tilde{g}(y) . \end{aligned} \quad (\text{A.7})$$

Another useful property of the Fourier transform concerns the derivatives,

$$\tilde{f}'(y) = \int \frac{df}{dx} \exp(ixy)dx = -iy \int f(x) \exp(ixy)dx = -iy \tilde{f}(y) . \quad (\text{A.8})$$

Fourier transforms for some simple cases can be expressed explicitly as follows:
shifted Dirac delta function $\delta_v(x) \equiv \delta(x-v)$

$$\tilde{\delta}_v(y) = \int \delta(x-v) \exp(ixy)dx = \exp(ivy) , \quad (\text{A.9})$$

Gaussian function $G_a(x) \equiv \exp(-x^2/a^2)$

$$\tilde{G}_a(y) = \int \exp(-x^2/a^2) \exp(ixy)dx = a\sqrt{\pi} \exp(-a^2y^2/4) . \quad (\text{A.10})$$

The Fourier transform can be easily generalized to complex functions on spaces of higher dimensions n

$$\tilde{f}(\vec{y}) = \int f(\vec{x}) \exp(i\vec{x}\vec{y})d^n x , \quad f(\vec{x}) = (2\pi)^{-n} \int \tilde{f}(\vec{y}) \exp(-i\vec{x}\vec{y})d^n y . \quad (\text{A.11})$$

Obviously, generalizing Eq. (A.4), a linear transform in \vec{x} space corresponds to an inverse transform in the \vec{y} space. In particular a rotation in a plane for an angle φ in one space corresponds to the rotation for $-\varphi$ in the other space. This is important for the Radon transform and its inverse.

A.2.2 Radon transform

Let us assume a function $f(x_1, x_2)$ in Cartesian coordinates in plane. Its perpendicular projection (in the direction of t -axis)

$$p(s, \varphi) \equiv \mathcal{R}[f](s, \varphi) = \int_{-\infty}^{\infty} f(s \cos \varphi - t \sin \varphi, s \sin \varphi + t \cos \varphi) dt \quad (\text{A.12})$$

to a line skewed for angle φ and parametrized by its length s is the Radon transform of f to variables $\{s, \varphi\}|_{s=-\infty}^{\infty}|_{\varphi=0}^{\pi}$. Obviously

$$p(s, \varphi + \pi) = p(-s, \varphi) , \quad (\text{A.13})$$

which is a condition for existence of f satisfying Eq. (A.12). In the case of Doppler tomography it means that the line profiles must be reversed in the opposite orbital phases if they result from a simple projection of the same velocity distribution of the emitting matter. For a fixed φ , the integral $p(s)$ is the zeroth Fourier mode in the variable t of the function $f(x_1, x_2)$ rotated into the coordinates s, t . This implies the so called Fourier slice theorem according to which the one-dimensional Fourier transform $\tilde{p}(u, \varphi) = \int p(s, \varphi) \exp(isu) ds$ of the Radon transform of $f(x_1, x_2)$ is a cross-section of the two-dimensional Fourier transform $\tilde{f}(y_1, y_2)$

$$\tilde{p}(u, \varphi) = \tilde{f}(u \cos \varphi, u \sin \varphi) . \quad (\text{A.14})$$

The existence theorem for inverse Radon transform follows from here, as well as a possibility how to reconstruct the two-dimensional distribution of the function $f(x_1, x_2)$ from a (sufficiently rich) set of its tomographic projections.

Back projection

The so called back-projection can be defined as

$$\mathcal{R}^*[p](x_1, x_2) = \int p(x_1 \cos \varphi + x_2 \sin \varphi, \varphi) d\varphi , \quad (\text{A.15})$$

which approximates (but it is not) the inverse Radon transform – obviously if the source is a single point

$$f = \delta(x_1 - s_0 \cos \varphi_0, x_2 - s_0 \sin \varphi_0) , \quad (\text{A.16})$$

then its projections are δ -functions shifted to follow an S-wave

$$p(s, \varphi) = \delta(s - s_0 \cos(\varphi - \varphi_0)) , \quad (\text{A.17})$$

but its back-projection reads

$$\mathcal{R}^*[p](x_1, x_2) = ((x_1 - s_0 \cos \varphi_0)^2 + (x_2 - s_0 \sin \varphi_0)^2)^{-\frac{1}{2}} . \quad (\text{A.18})$$

It means that it is peaked around the true position of the source f , but with a point-spread function inversly proportional to the distance from its centre. In a numerical application, where the integral $\int d\varphi$ in Eq. (A.15) is replaced by a sum over a finit number of available projections, the back-projection has a shape of a asterisk with rays in directions of individual projections. Yet \mathcal{R}^* is a good approximation to \mathcal{R}^{-1} for an iterative tomographic reconstruction.

Filtered back projection

Substituting for \tilde{f} from the Fourier slice theorem (A.14) into the inverse Fourier transform (A.11), we can reconstruct the image of f precisely in the form

$$f(\vec{x}) = (2\pi)^{-2} \int \tilde{p}(u, \varphi) \exp(-iu(x_1 \cos \varphi + x_2 \sin \varphi)) u du d\varphi . \quad (\text{A.19})$$

This integral in polar coordinates $\{u, \varphi\}$ in the plane of \vec{y} differs from the simple back-projection (A.15) by the presence of the multiplicator u at du , which is a filter suppressing the low-frequency modes of p and enhancing the high-frequency modes.

Iterative least-square technique

Suppose now that we have an object consisting of $N = N_1 \times N_2$ bins in coordinates (x_1, x_2) (labeled by index $i = (i_1, i_2)$), each one emitting with a rate f_i . This emission is registered in K_1 pixels of the variable s at each of K_2 tomographic projections in different angles φ (labeled by $k = (k_1, k_2)$), which detect a signal linearly dependent on the emission of source bins

$$p_k = \sum_i W_k^i f_i \quad (\text{A.20})$$

with some weighting factors W_k^i . Having an estimate of f_i , we solve for its correction Δ_i , which would minimize the least-square difference between the observed and calculated signal

$$0 = \delta \sum_k \left[p_k - \sum_i W_k^i (f_i + \Delta_i) \right]^2 \quad (\text{A.21})$$

with respect to any variation $\delta \Delta_j$. This condition yields

$$\sum_i \left(\sum_k W_k^j W_k^i \right) \Delta_i = \sum_k W_k^j \left[p_k - \sum_i W_k^i f_i \right] . \quad (\text{A.22})$$

Regarding Eq. (A.15), the solution of Eq. (A.20) can be approximated as

$$f_j \sim \sum_k W_k^j p_k = \sum_i \sum_k W_k^j W_k^i f_i , \quad (\text{A.23})$$

which means that

$$\sum_k W_k^j W_k^i \sim \delta_{ij} . \quad (\text{A.24})$$

Consequently, the solution of Eq. (A.22) with respect to the correction Δ_i can be estimated as

$$\Delta_j \simeq \frac{1}{\sum_k (W_k^j)^2} \sum_k W_k^j \left[p_k - \sum_i W_k^i f_i \right] . \quad (\text{A.25})$$

In practice, this estimate is multiplied by a damping factor $\epsilon < 1$ to prevent oscillations of the iterative procedure $f_i \rightarrow f_i + \epsilon \Delta_i$.

A.2.3 Moments of functions

For a function $f(x)$ its moments can be defined as

$$f_n \equiv \int x^n f(x) dx . \quad (\text{A.26})$$

For instance, for a Gaussian function $G(x) \equiv \exp(-x^2/a^2)$ (centered around $x = 0$)

$$G_{2n} = \frac{(2n)! a^{2n}}{n! 2^{2n}} G_0 , \quad G_{2n+1} = 0 . \quad (\text{A.27})$$

For convolution of two functions

$$\begin{aligned} (f * g)_n &= \int x^n f(x-y) g(y) dy dx = \sum_{k=0}^n \frac{n!}{(n-k)! k!} \int (x-y)^{n-k} f(x-y) dx y^k g(y) dy \\ &= \sum_{k=0}^n \frac{n!}{(n-k)! k!} f_{n-k} g_k . \end{aligned} \quad (\text{A.28})$$

If we define center of a function (representing, e.g., line-profile or a distribution function)

$$\bar{x}_f \equiv \frac{f_1}{f_0} , \quad (\text{A.29})$$

then

$$\bar{x}_{f*g} = \bar{x}_f + \bar{x}_g . \quad (\text{A.30})$$

Similarly, for a squared width of f defined by

$$\Delta_f^2 \equiv \frac{1}{f_0} \int (x - \bar{x})^2 f(x) dx = \frac{f_2}{f_0} - \bar{x}^2 , \quad (\text{A.31})$$

it is valid

$$\Delta_{f*g}^2 = \Delta_f^2 + \Delta_g^2 . \quad (\text{A.32})$$

Following Eq. (A.27), the fourth moment of the Gaussian function $G_4 = 3G_2^2/G_0$. If we characterize a non-Gaussianity of centered (i.e. $f_1 \equiv 0$) function f by ratio

$$R_f \equiv \frac{f_4 f_0}{3 f_2^2} \quad (\text{A.33})$$

(which is equal to 1 for Gaussian function), then

$$R_{f*g} = \frac{R_f \Delta_f^4 + R_g \Delta_g^4 + 2 \Delta_f^2 \Delta_g^2}{(\Delta_f^2 + \Delta_g^2)^2} . \quad (\text{A.34})$$

A.3 Manual for users of KOREL

A.3.1 Implementation of the code

The code KOREL is written in FORTRAN 77. It's PC-version (KOREL.FOR) includes on-line graphics (the package PHG.FOR), which is written for MicroSoft-fortran. The larger LINUX-version (KOREL.F) contains analogous package with graphical output to files (HPGL- or PS-) only and could thus be compiled by any fortran compiler. Starting from release of May 2004 the LINUX-version needs also the file KORELPAR.F, where the maximum number of spectra nsp and pixels (bins) $npix$ are given as parameters. Note that $npix2 = 2 * npix$ is also required as the array dimension for the complex representation of Fourier transforms of the spectra.

The code PREKOR for preparing the data for KOREL exists only in MS-version, because the use of on-line graphics is crucial for its use.

A.3.2 Controlling the run (file `korel.par`)

KOREL is controlled by the file `korel.par`, from which there are read (in free format, implicit fortran definition of type is valid):

1. Control keys

$$KEY(j)|_{j=1}^5, K0, IFIL, KR, KPR.$$

- Key $KEY(j)$ defines if the lines of the star No. j (according to Fig. 1.11) are present in the spectrum ($KEY(j) \geq 1$) or not. If $KEY(j)$ is split into digits $KEY(j) = 10 \times K_1 + K_0$, then $K_0 = 1$ means that the line-strength of the component j is fixed, while $K_0 = 2$ means that the intensity of this component is to be solved according to Eq. (1.44). $K_1 = 0$ means that the radial velocities of the component j are subjected to the orbital motion according to Eq. (1.97), while $K_1 = 1$ means that its radial velocities are free parameters, either fixed or converged.
- Key $K0$ specifies if there should be read data from the file `korel.dat` ($K0 > 0$), or if the calculation should go on with the previous data ($K0 = 0$), or (for $K0 < 0$) the number ($-K0$) of spectra is to be simulated.
- $IFIL$ is the number of harmonics to be removed by filtering.
- KR is the key of the form of graphic output `phg.out` ($KR = 0 \Rightarrow$ no output, $KR = 1 \Rightarrow$ PCX-format, $KR = 2 \Rightarrow$ PostScript-format).
- KPR controls the level of output. The value of KPR is to be split into digits, $KPR = 10 \times KPR_1 + KPR_0$. Then $KPR_0 > 1$ specifies that the information on simplex convergence has to be printed also into the file `korel.res`. $KPR_1 > 0$ specifies that the file `korel.o-c` has to be created, into which the difference spectra O – C will be written in the wavelength scale connected with the star No. KPR_1 (or in the original wavelength scale if $KPR_1 > 5$).

2. Next, there are read lines defining (initial) values of the free parameters, their (initial) steps for convergence etc. These lines have the form:

$$c, j, i, Kc, L1, L2, EL(j, i), \Delta(j, i) .$$

- Here the character c distinguishes the kind of the parameter and the indices 'j' and 'i' specify which one parameter of the kind is meant. The character c is equal either to 'o', 's', 'v', 'w' or 'e' (some other values are to be involved in future versions, other yet non-specified letters are interpreted as equivalent of 'o'). The letter 'o' stands for orbital parameter number $i|_{i=1}^{11}$ (cf. Table A.1) of orbit $j|_{j=0}^3$ (cf. Fig. 1.11). The letter 's' denotes the strength of lines of component (or telluric lines) j in the exposure number i , i.e. the natural logarithm¹ of the line-strengths, $EL(n) = \ln s_{ji}$. Similarly, 'v' denotes the velocity of component j in exposure i (for the case $KEY(j) \geq 11$) and 'w' enables to change the weight of exposure i (j being ignored). 'e' denotes scanning of $S(p)$ given by Eq. (1.32) in a two-dimensional cross-section of the p -space for calculation of errors of the orbital parameters specified by j and i like for the letter 'o'.
The output of these parameters has the same form (with explanation of meaning of the parameters at right on each line), so that the output values can be cut from `korel.res` and copied to the input file `korel.par` for next run of the code. The input of these lines is performed in a closed loop until a line with all values equal to zero is read (the letter may be arbitrary).
- $Kc > 0$ specifies if the above selected element is to be converged (or, for 'e', the scanning to be performed and saved in the output-file `korermap.dat`). The maximum of Kc for all elements gives the number of large iteration steps.
- Keys $L1, L2 > 0$ specify if the quantities $EL(n)$ and $\Delta(n)$ are to be read.
- $EL(n)$ and $\Delta(n)$ are the (initial) value of the element and its step (some numbers must be present even if they are ignored due to $L1 = 0$ and/or $L2 = 0$). In the case of letter 'e' these values are the half-widths of value intervals to be scanned on the x - and y - axis, resp.

3. If $K0 < 0$ then there are next read $-K0$ values of time, for which the data should be simulated. Next there must be given for each visible component its central intensity

¹This natural-logarithmic scale of strengths is close to the traditional magnitude-scale (because $\ln x \simeq 0.434 \times \log x$), however, a more positive value means a more intensive contribution of the component spectrum. These logarithmic values are normalized on output in their exponentials, i.e. $\sum_l s_{jl} = \sum_l 1$ (such a normalization in intensities seems to be more stable than that in (pseudo-)magnitudes, $\sum_l \ln s_{jl} = 0$, used in KOREL up to the year 2002).

Table A.1: Numbering of orbital elements

i	orbital element
1	P period [in days]
2	t_0 time of periastron passage [in days]
3	e eccentricity
4	ω periastron longitude [in degrees]
5	K semiamplitude of radial velocity of the component with the lower index [in km/s]
6	q the mass ratio of the component with the higher to that with the lower index
7	$\dot{\omega}$ the rate of periastron advance [in degrees/day]
8	\dot{P} the time derivative of the period
9	\dot{e} the time derivative of the eccentricity [in day ⁻¹]
10	\dot{K} the time derivative of K -velocity [in km/s/day]
11	\dot{q} the time derivative of mass ratio [in day ⁻¹]

c , its width Δ [km/s] and the code 1 or 2 specifying if the profile should be given by Eq. (1.105) or (1.106). Finally the noise of the spectrum and radial velocity per bin is read for the simulated data.

The following example of `korel.par` for the LINUX version:

```

1 1 0 0 2 1 0 2 2 | key(1,...,5), k= Nr. of sp., filter, plot, print
o 0 1 0 1 1 1.234567 0.000001 | sum= 9.8765
o 0 2 1 1 1 50001.000 .1 |
o 0 3 0 1 1 0.00 .1 |
o 0 4 0 1 1 90.00 1. |
o 0 5 1 1 1 120.0 .5 |
o 0 6 1 1 1 .5 .1 |
o 3 1 0 1 1 365.256360000 0.100 = PERIOD(3)
o 3 2 0 1 1 51547.520600000 10.000 = PERIASTRON EPOCH
o 3 3 0 1 1 0.016710220 0.001 = ECCENTRICITY
o 3 4 0 1 1 301.795199910 10.000 = PERIASTRON LONG.
o 3 5 0 1 1 0.001000000 0.000 = K1
o 3 6 0 1 1 0.000038185 0.000 = M2/M1, K2 = 26.188293833
o 3 7 0 1 1 0.000009111 0.000 = d omega/dt
o 3 8 0 1 1 0.000000000 0.100 = d P/dt
s 5 1 0 1 1 -0.15890 0.10000
s 5 2 0 1 1 0.07530 0.10000

```



```

s 5   3 0 1 1   0.10141 0.10000
s 5   4 0 1 1   0.20137 0.10000
s 5   5 0 1 1   0.18172 0.10000
s 5   6 0 1 1   0.04557 0.10000
s 5   7 0 1 1   0.05994 0.10000
s 5   8 0 1 1  -0.10638 0.10000
s 5   9 0 1 1  -0.17056 0.10000
x 0 0 0 0 0 0 0 | end of elements

```

will thus converge periastron epoch (identical with the maximum of radial velocity) and $K_{1,2}$ of a two-component binary (on circular orbit with period 1.234567 days) and solve for strengths of telluric lines (without filtering, with PS- output graphics and a detailed output protocol).

A.3.3 Input data (file `korel.dat`)

In the file `korel.dat` there is read the time [in Julian dates], initial wavelength [in Å], radial velocity per one bin [in km/s], the weight of each spectrum and (starting from release of 2003) also the number npx of pixels (bins) in each exposure.² It must be the same for all exposures and equal to 256 for the PC-version, while for the Unix-version it can be any multiple of 256 by number of the form 2^n , $n \geq 0$, up to the maximum value of npx defined by the parameter npx in the file `KORELPAR.F`. Next, there follow npx intensities in points with constant step in radial velocity. There can be read at maximum 27 input spectra for the PC-version or any number up to nsp defined in `KORELPAR.F` for the LINUX-version. These spectra are to be given in up to mnu spectral regions ($mnu = 5$ in the PC-version), each region being characterized by the initial λ and by the step of radial velocity per bin. Naturally, the number of input spectra in each region and their phase distribution must be sufficient for their decomposition, i.e. it must at least higher (or equal) than the number of calculated components. The number of decomposed spectra, i.e. the product of number of spectral regions \times number of components must not exceed the value $mnsu$ given together with npx , nsp and mnu in the file `KORELPAR.F` (or fixed to 15 in the PC-version).

The file `korel.dat` can be prepared by the code PREKOR.

A.3.4 The code PREKOR

The code PREKOR has been developed to facilitate the preparation of data for KOREL, it means to cut the proper spectral regions from a set of input spectra, to interpolate them

²A frequent mistake done by users is to run older versions of KOREL compiled for a fixed value of npx with data prepared for its different value. For this reason the value of npx is free in the newer LINUX versions, but it must be given in the data itself. The data without this value prepared by an older versions of PREKOR can be modified to the new form using the code 'KORTTRANS.F' (cf. Section A.3.6).

into the equidistant logarithmic wavelength scale and to write them in the format required by KOREL in the file `korel.dat`. Because a visual check of the proper choice of spectral regions is welcome, the PREKOR is written in MS-FORTRAN only and the distributed exe-version has to be run under DOS, even if the data are intended for a LINUX-version of KOREL. A version of PREKOR with PG-PLOT graphics is in preparation, however some problems with input of binary data makes it platform-dependent. Users without access to DOS- (or WINDOWS-) computers have to produce the `korel.dat` input using some other facilities (e.g. to select proper regions using MIDAS or IRAF and to rewrite them into the required format by some user-written code).

As an input, PREKOR needs a list of input spectra in file `prekor.lst` and it produces the data for KOREL in its (newly created) output file `prekor.out`, which has then to be renamed as `korel.dat`. Versions of PREKOR starting from October 2001 enable also to prepare parameters for disentangling the telluric lines, in which case an input file `prekor.par` is needed and the output is written as `prekor.res`.

When started, PREKOR asks the user at first to choose the mode of calculation (or the type of KOREL data to be got). The choice of *mode* = 0 performs the above mentioned calculation of parameters for disentangling of telluric lines. The choice *mode* > 0 means to prepare data with the number $npx = 128 \times 2^{mode}$ bins in each spectral region. It means that *mode* = 1 is required for the PC-version of KOREL, *mode* = 2 for the older LINUX-version and both or some higher integer number (up to a limit given by the array dimensions in the PREKOR code) can be chosen for the version with KORELPAR.F- file.

For *mode* > 0, PREKOR reads the description of files with individual exposures from the file `prekor.lst`. Older versions of PREKOR stopped after finishing the work with the first 30 spectra from `prekor.lst` and a rearrangement of this input file was needed to continue with the subsequent spectra (and to concatenate the corresponding output `prekor.out` files). Starting from versions of January 2004, PREKOR continues to cut out from subsequent spectra the region chosen according to the first displayed spectra and offers them for saving into output.

The file `prekor.lst` must contain on each line the name of file with individual exposure, its Julian date, weight, a code of the type of data file and the value of its shift in RV's (in the format `a12,f11.4,f8.3,i2,f8.3`). If the weight is negative, the data file is ignored.

The code = 0 denotes ASCII data files with wavelength and intensity in free format on each line; the first line is a comment.

The code =1 refers to files `*.rui` and

the code = 2 to `*.uui` of data in format SPEFO used formerly at Ondřejov observatory. The code =3 corresponds to the modified MIDAS output where the first three lines are a comment and then there follow lines with their sequence numbers (which are ignored by PREKOR), wavelengths and intensities.

The code = 4 means reading of tables produced by IRAF (with headings consisting of 106 records). Finally, for

the code =5, spectra in FITS- format (*BITPIX* = −32) can be read.

The dimensions of arrays in the code limit the length of the input spectrum to 4100 bins at maximum (the rest is ignored). The only exception are the input files in the FITS-format (code =5) where the preview of the whole spectrum is drawn using averaged pixel-values and the data used for the calculations are then read only starting from the required wavelength (the limit of 4100 pixels is thus valid for the chosen spectral region only). The first spectrum is read from its appropriate input file and its preview is plotted on the screen. User is asked to insert the initial wavelength and step in RV per bin. The corresponding spectral region is marked by a different colour on the wavelength scale and the chosen parts of spectra for the first portion of exposures (with non-negative weights) are then displayed to enable to check if their margins are really in the continuum. Later versions of PREKOR enable also an approximate rectification of the chosen spectral region consisting in normalization by linear function joining the first and the last pixel of the region.³ If the result is satisfactory, it can be saved into file **prekor.out** and subsequent spectral regions can be chosen in an infinite loop till the end of the run is not required.⁴ The final file **prekor.out** can then be renamed and used as **korel.dat**. The shift in RV of input spectra can be defined in the last column of **prekor.lst** either to transform the data from observed to heliocentric wavelength scale or to compensate for possible errors in wavelength-scale of the input spectra. These may be measured according to telluric lines either manually by some other mean or also by KOREL. A spectral region rich for telluric lines can be chosen first for this purpose and the column with O–C of RVs of telluric lines can be then copied from the file **korel.res** into **prekor.lst** to reduce the scatter of RVs of telluric lines in other spectral regions.

The theoretical RVs of telluric lines can be predicted from the coordinates of the observed star. To calculate the corresponding fictitious orbital parameters of the telluric lines (usually taken as the component No. 5 on the orbit No. 3), PREKOR can be run in mod = 0. In this case an additional file **prekor.par** must be prepared in which are given (on separate lines) the right ascension and declination of the star (in hours and minutes or degrees and arc-minutes, resp.). On next line, the equinox of the source coordinates is read. The following line gives the geographic longitude and latitude of the telescope in degrees and its altitude above the sea level in meters. As a result, a block of lines with orbital parameters of the orbit are written into the file **prekor.res**, from where they can be directly copied into **korel.par**. In addition, radial velocities of the telluric lines are calculated for each exposure listed in **prekor.lst** with higher precision taking into account also the planetary perturbations and the rotation of the Earth.

³This option can help for quick inspection of non-rectified spectra by preventing the jumps between the margins of the regions. However, its use may be dangerous because of hiding possible spectral lines on margins and because of the influence of random noise in the ultimate pixels. A thorough rectification of the whole spectrum before the run of PREKOR is always preferable.

⁴The commands for controlling the run of PREKOR differ depending on version, but they are always displayed on the screen and offered to the user.

A.3.5 The code REKTIF

In principle, the spectra of the components could be disentangled as absolute values of specific intensities I_ν in the whole range of frequencies ν , if the observed spectra are also given in the whole range as specific intensity with a sufficient precision.⁵ However, in practice, the observed spectra mostly cover only a small part of the whole spectral range and they are poorly calibrated in flux.⁶ The orbital Doppler shifts, which are of the order v/c , i.e., typically below 10^{-3} , are thus hardly discernible by observations of the whole spectra, but they can be better identified in relative shifts of spectral lines, the widths of which are often comparable or smaller than the amplitude of radial velocities. To investigate the Doppler shifts of spectral lines and to reduce the influence of uncertainties in the calibration of colour-dependence of spectrograph sensitivity, the so-called rectified spectra are used, i.e. the observed spectra normalized with respect to the estimated signal-value in continuum. From the point of view of physics of stellar atmospheres, the notion of continuum and hence also the procedure of rectification is spurious. The idealization of a continuum is useful if formation of a weak line on atoms immersed in background photon field is considered. In real atmosphere, however, the line-profiles often overlap and form the so-called pseudocontinuum.

For disentangling, the rectification enables to diminish the low Fourier modes, which can be influenced by the above mentioned sensitivity effects, and it also removes (or decreases) possible jumps between the left and right margin of each spectral region, which could give rise to some unevenness on edges. From this point of view, it is not much important if the continuum is chosen for the rectification at a proper level. What matters is at first the scale of wavelengths, on which the continuum varies, and also its consistency for all observed spectra. The scale of continuum variations should be larger compared to the searched Doppler shifts and characteristic scales of spectral features (lines) used to reveal the shifts. The rectification should remove such large-scale variations. If it fails to do it correctly or even if it introduces such variations, the disentangling may produce an artifact in form of long-scale distortions or waves in the continuum of component spectra. These distortions caused by unreliable rectification may even prevail in the O–C over the true orbital changes of the spectra and the solution of orbital parameters may fail in order to use these degrees of freedom in favour of correcting the wrong rectification. The danger of this failure can be escaped or minimized by filtering the low Fourier modes.

A common way of rectification is to draw the continuum in the form of spline function defined by interactively chosen points (e.g. in the code SPEFO, cf. Škoda 1996; like in SPEFO, the splines are calculated in REKTIF according to G. Hill, 1982). This

⁵In fact, this was the original Doppler's idea to explain observed colour differences between components of some binaries by their frequency shifts due to radial velocities. Despite the effect of colour changes is practically negligible for usual binaries, it exists and in principle its phase-dependence can enable to disentangle individual component's colours. Cf. A.1 at p. 201

⁶This problem is particularly difficult for echelle spectra, where also a smooth connection of subsequent orders is a non-trivial task.

‘artistic’ procedure depends on a skill of user and cannot be homogeneously repeated in different spectra. To make it a bit more reliable, the code REKTIF was written by the author for preparing the data for KOREL. In this code, the marks defining the continuum are recurrently improved. Starting with a set of marks with chosen wavelengths and intensities, new mean values of both these quantities are calculated for all data-points in the observed spectrum, which fall into a wavelength interval of predefined width around each mark and the intensities in which fit with the present spline approximation of the continuum within a precision limit chosen in a percentage of the continuum. The limit then shrinks down slowly (by a geometric sequence typically with quotient about 0.8) in subsequent iterations, so that the intensity attributed to each mark converges to the mean of the most populated (rectified) intensity values. These are supposed to correspond to the (pseudo-)continuum, while the data-points in lines within the interval are skipped from the mean, when the limit decreases to the level of signal noise. An experience shows, that this algorithm gives mostly a result consistent with the ‘artistic insight’, however, it is recommended to check the result in a graphic form to improve the cases when more marks are needed or when some of them converge to a wrong value of intensity (this can happen due to inconvenient initial approximation).

The input spectrum to be rectified is read by the code REKTIF from a file named **rektif.dat**. It is to be given in a form of table with wavelength in the first and the intensity in the second column. The number of lines should not exceed the value of parameter *NPXM* chosen at the beginning of the code source-file. The table may contain several lines of comments at the top, the number *NTXT* of which is to be given together with other parameters controlling the run of the code. These parameters are read from file **rektif.par**. The first line should give subsequently λ_{min} , λ_{max} , I_{min} , I_{max} (i.e. the window to be displayed) and *NTXT*. Next line gives number *NR* of marks ($NR \leq NRM$ also set as a parameter in the code), number of iteration steps and a quotient q by which the range of acceptable errors of intensity is shrunk in each iteration (value $q \simeq 0.9$ is proved in practice). Then initial values of λ , I , $\Delta\lambda$ and maximum $\delta I/I_{cont.}$ are given for each mark on a separate line. The resulting rectified spectrum is given in the file **rektif.out** and improved values of marks in the file **rektif.res** (the additional fifth column gives the number of points taken into account for each mark).

A.3.6 The code KORTTRANS

This code was originally written to transform the file **korel.dat** from DOS to UNIX format on computers, where the utility DOS2UNIX is not available. The code PREKOR writes intensities for each exposure by one command – always 10 values in one line ended by mark nonunderstandable to UNIX. The code KORTTRANS can read each line separately from these files renamed to **kortrans.in** and to write them into **korel.dat** directly readable by KOREL. Because the older version of KOREL did not require the number *npx* of bins in the heading of each exposure, KORTTRANS can update the old data by

inserting this value given in file `kortrans.par`. This file has a single line with values npx , v_1 , v_2 , Δv in a free format (e.g. “512 0.02 0.98 0.005”). If the value $dv > 0$, the spectral region of each input exposure is transformed (filtered or tapered at edges – Section 1.6.2, p. 29) according to formula

$$I_{out}(v) = 1 + (I_{in}(v) - 1) / (1 + \exp \frac{v_1 - v}{\Delta v}) / (1 + \exp \frac{v - v_2}{\Delta v}) , \quad (\text{A.35})$$

where v is the logarithmic wavelength rescaled to be 0 and 1 on both edges of the spectral regions. This tapering suppresses smoothly (on a characteristic width Δv) spectral lines and deviations of continuum from 1 at edges of the spectral region (i.e. below v_1 and above v_2).

A.3.7 Input data (file `korel.tmp`)

The template spectra for constrained disentangling as described in the Section ?? may be read in the file `korel.tmp`. The data should have the form:

```
6510. 5. 5
1.0014
1.0021
0.9993
1.0006
...
```

Here the first two numbers in the first line define (in the same way as in the `korel.dat`) the spectral region for which the template is prepared and the last digit gives the number of component which should have this spectrum. Next lines give the values of the intensity (in free format, it means there may be more of them on the same line) for each grid point of the input spectra.

A.3.8 Outputs of KOREL

There are several possible forms of output. During the run of the code a basic information is shown on the screen. In the PC-version this information includes graphical output on the screen. Simultaneously, the figure can be written into the file `phg.out`.⁷ Main information about the run and the results is contained in the file `korel.res`. Residual spectra can be stored in the file `korel.o-c`.

After the input of the data and control keys, the basic information on the task (e.g. the number of data and number of parameters to be solved) is summarized on the screen. Then the input spectra are drawn in green colour (in the PC-version) subsequently from

⁷To facilitate the next work with the graphics output, it is named `phg.ps` in the case of PostScript format.

the top to the bottom of the screen. During the iteration of parameters, a protocol on the simplex procedure is shown on the screen and it can be directed also to `korel.res`.⁸ In this protocol, the first number indicates the step (running up to ten times the number of iterated parameters), letter A, B, C or D shows the type of simplex operation and the following number the worst point of the simplex (which is to be improved).⁹ It is recommended to check if the first point is improved reasonably soon. The opposite may indicate that there was chosen a too large initial value of step of some parameter (usually of that, which is improved first). Next in the line is written the highest value of the minimized sum. It should be decreasing, however an increase is possible at the shrinkage operation indicated by D.¹⁰ Next there are typed the values of converged parameters, which help to check the status of the convergence. After the end of the convergence, the disentangled line profiles are shown at the bottom of the screen in blue colour and their superpositions with velocities corresponding to the solution of orbital parameters are plotted in blue over the green input spectra. Finally, each spectrum is fitted by the superposition of disentangled profiles with RVs independent of the orbital parameters and the corresponding fit is drawn in red. The L-shaped line in the figure indicates the wavelength unit (100km/s) and the unit of intensity (0.1 of the continuum level).

The file `korel.res` yields most of the information about the calculation and its results. First, there are summarized the values of parameters characterizing the input of the task like the number of spectra etc. Next, during the iteration, there is written in each its step the number of the step, the value of the sum S of squares for the present values of orbital parameters, its value after recalculation of the strengths of lines and the mean error of the intensity. If the print-mode is ≥ 2 , the protocol on the convergence by simplex-method is copied here as well. After the iteration, the orbital parameters are printed for each orbit with non-zero period. Next, all non-zero strengths of lines are printed together with the final values of their steps (which can be changed with respect to their input values if the corresponding parameters have been converged by simplex). Then the values of S are repeated once more. Next the spectra of individual components are printed (in the order of columns corresponding to the order of component stars). It must be kept in mind, that the values of continua of individual components are unknown, so that the depths of lines are normalized with respect to the sum all continua. The number 1.0 is added to each component spectrum to prevent the negative values in absorption profiles. Each spectral region is introduced by information on the number of exposures contributing to it and by the mean value of their shifts of continua. Finally, for each exposure the radial velocities found as the best superposition of the decomposed spectra are printed. The order of the components corresponds to the previously used order of the output spectra

⁸Cf. the use of key *KPR* in Section A.3.2.

⁹See the FOTEL-manual (Hadrava 2004b) for a more detailed explanation of the protocol and its meaning.

¹⁰Obviously, the monotonous decrease of the sum can also be violated by an insufficient convergence of the line strengths (as explained on page 1.6.11).

and, in addition, it is indicated by the number of the component. Each radial velocity is followed by the value of O–C, where C corresponds to the value according to the final values of orbital parameters.

The file `korermap.dat` provides a matrix of 20×20 values of the $(O-C)^2$ scanned at a two-dimensional cross-section of the space of orbital parameters. This matrix may be read and the dependence drawn by the code ISOLIN.

A.3.9 The code KORNOR

To facilitate the normalization of spectra disentangled by KOREL a simple code named KORNOR has been written (in MS-Fortran). This code reads the parameters *par*, *mi*, *np_x*, *np_y* and *kr* from the first line and $C_j|_{j=1}^{np}$ from the second line of the file `kornor.par` and the disentangled spectra cut out from the file `kornor.dat` in the form of table $\lambda_i, I'_{1,i}, \dots, I'_{np,i}|_{i=1}^{np_x}$ (for each spectral region separately). KORNOR draws first these input spectra on the screen in pale colours and with the unknown continua shifts as they are received from KOREL (i.e. the mean intensity shifted to the level = 1). It also draws (in yellow colour) an example composed spectrum with zero Doppler shifts of components and the proper shift of the continuum given by the parameter *mi* which is the mean intensity given for each spectral region in the output of KOREL. The continuum is then identified in this spectrum and marked by red line at the level = 1. It is defined to be in frequencies where the spectrum differs from 1 for less than a multiple *par* (which has to be established by the method of trials and errors, but typically can be chosen around 0.2) of the noise of the spectrum. At these points the integrals at continua of each component are calculated and the continuum shifts are found according to Eq. (1.94). The rectified component spectra are finally rescaled, i.e. calculated by Eq. (1.96) using continua values C_j given at the file `kornor.par` and they are drawn on the screen and written on the output.

A.3.10 Problems with KOREL

In this Section some hints, explanations to problems and answers to often asked questions of users will be given.

Incomprehensible list input in korel.dat: This error message and abort at the beginning of the run of KOREL appears when the file `korel.dat` is prepared by PREKOR on a DOS operating computer and it is transmitted to a LINUX operating computer for the run of KOREL. It is due to the incompatibility of the ends of lines between these systems. It can be corrected using the utility DOS2UNIX on the file `korel.dat` or using the code KORTTRANS, which can yield some additional corrections to the input data.

Array bounds exceeded in subroutine CSWAP: This subroutine is called to exchange two columns of a matrix in the solution of a set of linear equations by the subroutine CGSEV accepted from the LAPACK package of FORTRAN routines. It uses a standard

trick to speed up matrix operations avoiding the lengthy straightforward calculation of position in computer memory for each element of a multidimensional array by a use of its equivalence with a vector. The dimension of this vector is declared only formally in this subroutine (and it is underestimated) and the proper bound of the array is ensured by the correct demands of the higher subroutine. Array bounds checking of the FORTRAN compiler should thus be switch off.

Undulation of disentangled spectra: Sometimes it happens that the disentangled spectra have large amplitude and long wavelength wavy perturbations in antiphase (which cancel in the sum of all components). Such errors appear quite often at the beginning of the spectra decomposition and in favourable case (but not always) they are suppressed in the course of convergence of the orbital and other free parameters. This feature is due to a bad definition of lower Fourier modes by Eq. (1.32); the continua of components cannot be distinguished, because they are not affected by the orbital motion at all, and the lower modes are affected only slightly, hence they are determined only poorly — the corresponding matrix is nearly singular and a small error (e.g. in rectification of input spectra) can result in exaggerated values of amplitudes of the modes. This danger increases if the disentangled regions are long compared to the real RV- amplitudes. The contributions of these poorly determined modes to the total minimized sum S can be still small, so that the solution of higher Fourier modes and the free orbital and others parameters can be still correct. In such a case, it is sufficient to rectify the disentangled spectra once more.¹¹ However, there is a real danger that the RVs or line-strengths will converge to a false minimum in which the source of the low modes will be fitted best and the true spectral lines encrypted in higher modes will be ignored. Several actions can be undertaken to prevent this failure. Firstly, user should check if all exposures are correctly rectified¹² and either to improve or to remove suspicious exposures. The use of filtering out the lower modes (by the key *IFIL* described in Section A.3.2) may help to hit the proper solution, in which finally also the undulation may be suppressed. A better initial estimate of orbital parameters or line-strengths (e.g. from other spectral regions, from some other sources or simply found by chance from numerous trials) may also be helpful.

¹¹A simultaneous rectification of all components at once with the condition of mutual cancelling of the corrections would be desirable.

¹²Problems may arise also from overlaps of orders in echelle spectra.

A.4 List of objects studied with Fourier disentangling

The following list gives observational papers, in which the Fourier disentangling is cited, which mostly means that their results were achieved with KOREL, but in some cases also that the authors failed in its use. In both cases these papers may be of some interest for future studies of the same or similar systems.

A&A 309, 521 (96)	55 UMa	ASCP 318, 338 (04)	HD 140873, HD 123515
A&A 315, L401 (96)	β Cep	ASCP 318, 342 (04)	DG Leo
A&A 319, 867 (97)	V436 Per	IAUS 215, 166 (04)	66 Oph
A&A 322, 565 (97)	β Sco	IAUS 224, 923 (04)	α Dra, HD 116656
A&A 327, 551 (97)	4 Her	MNRAS 349, 547 (04)	V615 Per, V618 Per
ARep 41, 630 (97)	o Per	A&A 432, 955 (05)	κ Sco
CoSka 27, 41 (97)	AR Aur	A&A 439, 309 (05)	V578 Mon
ARep 42, 312 (98)	V373 Cas	A&A 440, 249 (05)	ε Lup
A&A 331, 550 (98)	χ^2 Aur	ApJ 623, 411 (05)	TT Hyd
A&A 332, 909 (98)	SZ Cam	ApSpSc 296, 169 (05)	o And
A&A 345, 531 (99)	V606 Mon	ApSpSc 296, 173 (05)	κ Dra
A&A 345, 855 (99)	AR Cas	ASCP 333, 211 (05)	55 UMa
A&A 353, 1009 (00)	β Lyr	MNRAS 356, 545 (05)	DG Leo
A&A 358, 553 (00)	V578 Mon	A&A 446, 583 (06)	ε Per
ASCP 214, 697 (00)	β Lyr	A&A 455, 1037 (06)	V360 Lac
IAUS 200, 109 (00)	V578 Mon	A&A 455, 259 (06)	β Cen
A&A 366, 558 (01)	QZ Car	CoAst 148, 65 (06)	θ^2 Tau
A&A 377, 104 (01)	ψ^2 Ori	MNRAS 370, 884 (06)	λ Sco
AJ 123, 988 (02)	o Leo	MNRAS 370, 1935 (06)	δ Lib
ApJ 564, 260 (02)	HV 982 (LMC)	A&A 463, 1061 (07)	V379 Cep
ApJ 574, 771 (02)	EROS 1044 (LMC)	ApJ 463, 579 (07)	HD 23642
MNRAS 330, 288 (02)	α Equ	ApJ 464, 263 (07)	HD 110555
A&A 405, 1087 (03)	V497 Cep	ASCP 361, 482 (07)	β Per
A&A 408, 611 (03)	V436 Per	MNRAS 382, 609 (07)	η Mus
ApJ 587, 685 (03)	HV 5936 (LMC)	arXiv 0710.0758 (07)	Cyg X-1
A&A 419, 607 (04)	κ Dra	A&A 481, 183 (08)	V1007 Sco
A&A 422, 1013 (04)	κ Sco	AJ 136, 631 (08)	Cyg X-1
A&A 427, 581 (04)	λ Sco	ApJ 678, (08)	Cyg X-1
A&A 427, 593 (04)	λ Sco	ESO AS 67 (08)	HD 208905
ASCP 318, 103 (04)	b Per	MNRAS 385, 381 (08)	V716 Cen
ASCP 318, 114 (04)	RV Crt		

Bibliography

- [1] Albrecht S., Reffert S., Snellen I., Quirrenbach A., Mitchell D.S. 2007, A&A 474, 565: “The spin axes orbital alignment of both stars within the eclipsing binary system V1143 Cyg using the Rossiter Mc Laughlin effect”
- [2] Bagnuolo W. G. Jr., Gies D. R. 1991, ApJ 376, 266-271: “Tomographic separation of composite spectra: The components of the O-star spectroscopic binary AO Cassiopeiae”
- [3] Bagnuolo W. G. Jr., Gies D. R., Hahula M. E., Wiemker R., Wiggs M. S. 1994, ApJ 423, 446-455: “Tomographic separation of composite spectra. II. The components of 29 UW Canis Majoris”
- [4] Butler R. P. 1993, ApJ 415, 323-334: “Cepheid velocity curves from lines of different excitation and ionization. I. Observations”
- [5] De Cuyper J.-P., Hensberge H. 2002, “Improving the Rectification of Echelle Spectra”, in: *Astronomical Data Analysis Software and Systems XI*, D. A. Bohlender, D. Durand and T. H. Handley (eds.), ASP Conf. Ser. 281, 324-327
- [6] Doppler Ch. 1842, Abhandlungen der königliche böhmischen Gessellschaft der Wissenschaften 2, 465-482: “Über farbige Licht der Doppelsterne und einiger anderer Gestirne des Himmels”
- [7] Ferluga S., Floreano S., Mangiacapra D. 1991, La Lettre de l’OHP 6, 3: “Aurélien for detecting double-line eclipsing binaries”
- [8] Ferluga S., Floreano S., Bravar U., Bédalo C. 1997, A&AS 121, 201-209: “Separating the spectra of binary stars”
- [9] González J. F., Levato H. 2006, A&A 448, 283-292: “Separation of composite spectra: the spectroscopic detection of an eclipsing binary star”
- [10] Gray D. F. 2005, “The observation and analysis of stellar photospheres” (Third edition), Cambridge University Press
- [11] Griffin R. F. 1967, ApJ 148, 465-476: “A photoelectric radial-velocity spectrometer”
- [12] Griffin R. F. 1975, The Observatory 95, 23-27: “Spectroscopic binary orbits from photoelectric radial velocities”
- [13] Hadrava P. 1990, Contrib. Astron. Obs. Skal. Pl. 20, 23-25: “Eclipsing Binaries – Light-curve solution”
- [14] Hadrava P. 1991, “FOTEL – User’s guide” (electronic document), Astron. Inst. ČSAV

- [15] Hadrava P. 1995, A&AS 114, 393-396: “Orbital elements of multiple spectroscopic stars”
- [16] Hadrava P. 1997, A&AS 122, 581-584: “Relative line photometry of eclipsing binaries”
- [17] Hadrava P. 2001a, “The method of spectra disentangling and its links to Doppler tomography”, in: *Astrotomography, indirect imaging methods in observational astronomy*, H. M. J. Boffin, D. Steeghs, J. Cuypers (eds.), Lecture notes in physics vol. 573, pp. 261-268, Springer
- [18] Hadrava P. 2001b, “Spectroscopy of binaries”, DSc. thesis (in Czech), Astronomical Institute ASCR, Ondřejov
- [19] Hadrava P. 2003, “Spectroscopy of binary stars”, in: *New directions for close binary studies: The royal road to stars*, O. Demircan, E. Budding (eds.), Publ. COMU Ap. Research Center, Vol. 3, pp. 84-90
- [20] Hadrava P. 2004a, “Disentangling of spectra of multiple stars”, in: *Spectroscopically and spatially resolving the components of the close binary stars*, R. W. Hilditch, H. Hensberge, K. Pavlovski (eds.), ASP. Conf. Ser. 318, pp. 86-94
- [21] Hadrava P. 2004b, Publ. Astron. Inst. ASCR 92, 1-14: “FOTEL4 – User’s guide”
- [22] Hadrava P. 2004c, Publ. Astron. Inst. ASCR 92, 15-35: “KOREL – User’s guide”
- [23] Hadrava P. 2005, Astrophys. & Sp. Sc. 296, 239-249: “New techniques and limitations of light curve analysis”, in: “Zdeněk Kopal’s Binary Star Legacy”, eds. H. Drechsel and M. Zejda, Springer
- [24] Hadrava P. 2006a, A&A 448, 1149-1152: “Disentangling telluric lines in stellar spectra”
- [25] Hadrava P. 2006b, Astrophys. Sp. Sc. 304, 337-341: “Disentangling of the Spectra of Binary Stars – Principles, Results and Future Development”
- [26] Hadrava P. 2007a: “New trends in disentangling the spectra of multiple stars”, in: Proceedings IAU Symp. 240, 111
- [27] Hadrava P. 2007b: “Line profiles during eclipses of binary stars”, in: “Solar and stellar physics through Eclipses”, O. Demircan, S. O. Selam and B. Albayrak eds., ASP Conf. Ser. 370, 164-168
- [28] Hadrava P. 2009: “Notes on the disentangling of spectra. I. Enhancement in precision”, A&A 494, 399-402
- [29] Hadrava P., Kubát J. 2003, “Limb Darkening and Line-profile Variations in Eclipsing Binaries”, in: *Workshop on Stellar Atmosphere Modeling*, I. Hubeny, D. Mihalas, K. Werner (eds.), ASP Conf. Ser. 288, pp. 149-152
- [30] Hadrava P., Šlechta M., Škoda P. 2009: “Notes on the disentangling of spectra. II. Intrinsic line-profile variability due to Cepheid pulsations”, A&A, in press
- [31] Heinzel P., Hadrava P. 1975, BAIC 26, 90-91: “Precise Measurement of Radial Velocity Using a LIREPHO Microphotometer”

- [32] Hensberge H. 2004, “Do our spectra match the requirements for a precise analysis of SB2s?”, in: *Spectroscopically and spatially resolving the components of the close binary stars*, R. W. Hilditch, H. Hensberge, K. Pavlovski (eds.), ASP. Conf. Ser. 318, pp. 43-51
- [33] Hensberge H., Ilijić S., Torres K.B.V. 2008, A&A 482, 1031: “On the separation of component spectra in binary and higher-multiplicity stellar systems: bias progression and spurious patterns”
- [34] Hill G. 1982, Publ. DAO XVI, 67: “Intep – an effective interpolation subroutine”
- [35] Hill G. 1993: “The measurement of radial velocities using cross-correlation technique as applied to binary stars”, in: *New Frontiers in Binary Stars Research*, K.-C. Leung, I.-S. Nhu (eds.), ASP. Conf. Ser. 38, pp. 127-153
- [36] Holmgren D. 2004, ASP Conf. Ser. 318, 95-102: “Improvement of spectroscopic binary star orbits through the use of spectral disentangling”
- [37] Hossack W. R. 1952, AJ 57, 15: “An oscilloscopic microphotometer and plate measuring machine”
- [38] Hynes R. I., Maxted P.F.L. 1998, A&A 331, 167-170 “A critique of disentangling as a method of deriving spectroscopic orbits”
- [39] Ilijić S., Hensberge H., Pavlovski K. 2001: “Fourier disentangling of composite spectra”, in: *Astrotomography, indirect imaging methods in observational astronomy*, H. M. J. Boffin, D. Steeghs, J. Cuypers (eds.), Lecture notes in physics vol. 573, pp. 269-275, Springer
- [40] Kallrath J., Linnell A. P. 1987, ApJ 313, 346-357: “A new method to optimize parameters in solutions of eclipsing binary light curves”
- [41] Kallrath J., Milone E. F. 1999, “Eclipsing binary stars: modeling and analysis”, Springer-Verlag, New York, Berlin
- [42] Liu N., Gies D. R., Xiong Y., Riddle R. L., Bagnuolo W. G. Jr., Barry D. J., Ferrara E. C., Hartkopf W. I., Hooda J.S., Mason B.D., McAlister H.A., Roberts L. C. Jr., Sowers J. W. 1997, ApJ 485, 350-358: “Tomographic separation of composite spectra. V. The triple star system 55 Ursae Majoris”
- [43] Marchenko S. V., Moffat A. F. J., Eenens P. J. R. 1998, PASP 110, 1416-1422: “The Wolf-Rayet binary WR 141 (WN5o + O5 V-III) revisited”
- [44] Marsh T. R., Horne K. 1988, MNRAS 235, 269-286: “Images of accretion discs – II. Doppler tomography”
- [45] McLaughlin D. B. 1924, ApJ 60, 22-31: “Some results of a spectrographic study of the Algol system”
- [46] Minaroviech M., Zverko J., Žižňovský J. 1984, “TV-Abbe comparator”, in: *Magnetic stars*, p. 106
- [47] Lindegren L., Dravins D. 2003, A&A 401, 1185-1201: “The fundamental definition of “radial velocity””
- [48] Ohta Y., Taruya A., Suto Y. 2005 ApJ 622, 1118

- [49] Piskunov N. E., Valenti J. A. 2002, A&A 385, 1095-1106: “New algorithms for reducing cross-dispersed echelle spectra”
- [50] Rossiter R. A. 1924, ApJ 60, 15-21: “On the detection of an effect of rotation during eclipse in the velocity of the brighter component of beta Lyrae, and on the constancy of velocity of this system”
- [51] Rucinski S. 1992, AJ 104, 1968-1981: “Spectral-line broadening functions of WUMa-type binaries. I. AW UMa”
- [52] Rucinski S. 2002, AJ 124, 1746-1756: “Radial velocity studies of close binary stars. VII. Methods and uncertainties”
- [53] Schlesinger F. 1909, Publ. of Allegheny Obs. 1, 123-134: “The Algol-variable δ Lybrae”
- [54] Simkin S. M. 1974, A&A 31, 129-136: “Measurements of velocity dispersions and Doppler shifts from digitized optical spectra”
- [55] Simon K. P., Sturm E. 1994, A&A 281, 286-291: “Disentangling of composite spectra”
- [56] Simon K. P., Sturm E., Fiedler A. 1994, A&A 292, 507-518: “Spectroscopic analysis of hot binaries II. The components of Y Cygni”
- [57] Škoda P. 1996: “SPEFO – a simple, yet powerful program for one-dimensional spectra processing”, in: *Astronomical Data Analysis Software and System V*, G. H. Jacoby, J. Barnes (eds.), ASP. Conf. Ser. 101, pp. 187-190
- [58] Škoda P., Šurlan B., Tomić S. 2008, in preparation
- [59] Stickland D. J. 1997, The Observatory 117, 37-50: “Three massive binaries and the ‘Struve-Sahade’ effect”
- [60] Sturm E., Simon K. P. 1994, A&A 282, 93-105: “Spectroscopic analysis of hot binaries I. The components of DH Cephei”
- [61] Townsend R. H. D. 1997, MNRAS 284, 839-858: “Spectroscopic modelling of non-radial pulsation in rotating early-type stars”
- [62] Walker G.A.H., Yang S., Fahlman G.G. 1979, ApJ 233, 199-204: “Spectral variations in ζ Ophiuchi related to rotation?”
- [63] Zucker S., Mazeh T. 1994, ApJ 420, 806-810: “Study of spectroscopic binaries with TODCOR. I. A new two-dimensional correlation algorithm to derive the radial velocities of the two components”
- [64] Zucker S., Mazeh T. 2006, MNRAS 371, 1513-1518: “TIRAVEL – Template-Independent RAdial VELOCITY measurement”
- [65] Zucker S., Torres G., Mazeh T. 1995, ApJ 452, 863-869: “Study of spectroscopic binaries with TODCOR. III. Application to triple-lined systems”

Program of the Summer School

Monday 15. 9.

- 9:00 - 12:00 P. Hadrava: Introduction into disentangling
- 12:00 - 14:00 lunch
- 14:00 - 18:00 Exercises
- 18:00 - Wellcome party

Tuesday 16. 9.

- 9:00 - 10:20 P. Hadrava: Related spectroscopic methods
- 10:40 - 12:00 P. Hadrava: Advanced disentangling
- 12:00 - 14:00 lunch
- 14:00 - 14:30 H. Lehmann: TW Dra – Spectral disentangling of an unusual triple system
- 14:30 - 15:00 H. Ak: KOREL application on spectroscopic binary HD 10308
- 15:00 - 18:00 Exercises

Wednesday 17. 9.

- 9:00 - 10:20 P. Hadrava: Preparation of spectra for disentangling
- 10:40 - 12:00 P. Škoda: Spectra reduction related problems of Fourier disentangling
- 12:00 - 14:00 lunch
- 14:00 - 14:30 N. F. Ak: KOREL application on spectroscopic binary IX Per
- 14:30 - 15:00 H. V. Senavci et al.: The Echelle Spectra of SW Lac
- 15:00 - 18:00 Exercises

Thursday 18. 9.

- 9:00 - 10:20 P. Hadrava: Results from KOREL
- 10:40 - 12:00 J. Kubát: Model atmospheres and synthetic spectra
- 12:00 - 14:00 lunch
- 14:00 - 14:30 O. Creevey: Spectroscopic observations of a red-edge delta Scuti star in an eclipsing binary
- 14:30 - 18:00 Exercises

Friday 19. 9.

- 9:00 - 10:20 P. Hadrava: Future of disentangling
- 10:40 - 12:00 P. Škoda: Futuristic vision of spectra disentangling in the new milenium (focus on GRID computing, Virtual Observatory, Workflows, Web services)
- 12:00 - 14:00 lunch
- 14:00 - 16:00 Closing discussion

List of participants

Hasan Ak	hasanak@erciyes.edu.tr (Kayseri Turkey)
Nurten Filiz Ak	(Kayseri Turkey)
Eva Arazimová	arazimova@sunstel.asu.cas.cz (Ondřejov, Czech Rep.)
Omur Cakirli	omur.cakirli@gmail.com (Izmir, Turkey)
Orlagh Creevey	orlagh@iac.es (Spain)
Attila Cseki	attila@aob.bg.ac.yu (Serbia)
Dominik Drobek	drobek@astro.uni.wroc.pl (Wroclav, Poland)
Jan Elner	janelner@centrum.cz (Ondřejov, CR)
Pedro Amado Gonzalez	pja@iaa.es (Granada, Spain)
Lubomir Hambalek	lhambalak@ta3.sk (Slovakia)
Saskia Hekker	Saskia.Hekker@oma.be (Belgium)
Baju Indradjaja	bindra@physics.muni.cz (Indonesia)
Emil Kundra	ekundra@ta3.sk (Slovakia)
Patricia Lampens	patricia.lampens@oma.be (Brussel, Belgium)
Olivera Latkovic	olatkovic@aob.bg.ac.yu (Serbia)
Holger Lehmann	lehm@tls-tautenburg.de (Jena, Germany)
Joanna Molenda-Zakowicz	molenda@astro.uni.wroc.pl (Wroclav, Poland)
Andrzej Pigulski	pigulski@astro.uni.wroc.pl (Wroclav, Poland)
Jan Polster	hans@algieba.asu.cas.cz (Brno, Czech Republic)
Volkan Senavci	volkan@astro1.science.ankara.edu.tr (Ankara, Turkey)
Tamas Szalai	szaszi@titán.physx.u-szeged.hu (Szeged, Hungary)
Staszek Zola	zola@astro1.as.ap.krakow.pl (Krakow, Poland)
Melike Afsar	(Izmir, Turkey)
Zeynep Bozkurt	(Izmir, Turkey)
David Holmgren	holmgrenm@shaw.ca (Kanada)
Somaya Saad	somaya111@yahoo.com (Egypt)
Faruk Soyduğan	fsoydugan@comu.edu.tr (Canakkale, Turkey)

